Conformational Modulation and Polymerization-Induced Folding of Proteomimetic Peptide Brush Polymers

Julia Oktawiec,[a] Omar Ebrahim,[a] Yu Chen,[b] Kaylen Su,[c] Christopher Sharpe,[b] Nathan D Rosenmann,[b] Clara Barbut,[a] Steven Weigand,[d] Matthew Thompson,[a] James Byrnes,[e] Baofu Qiao,[c] Nathan Gianneschi[a,b,f]

Author Affiliations:
[a] Department of Chemistry, Northwestern University, Evanston, IL 60208
[b] Department of Materials Science and Engineering, Northwestern University, Evanston, IL 60208
[c] Department of Natural Sciences, Baruch College, City University of New York, New York, NY 10010
[d] DuPont−Northwestern−Dow Collaborative Access Team (DND-CAT) Synchrotron Research Center, Northwestern University, Argonne, IL 60208
[e] Beamline 16ID, NSLS-II, Brookhaven National Laboratory, Upton, NY, 11973
[f] International Institute for Nanotechnology, Chemistry of Life Processes Institute, Simpson Querrey Institute, Lurie Cancer Center, Department of Biomedical Engineering, and Department of Pharmacology, Northwestern University, Evanston, IL 60208

1. Materials

All amino acids used to prepare peptides by solid-phase peptide synthesis (SPPS) were obtained from commercial sources. Lithium chloride (99%) and 6-Fmoc-amino hexanoic acid (97%) were purchased from commercial sources and used without purification. N-(hexanoic acid)-cis-5-norbornene-exo-dicarboximide and the olefin metathesis initiator $(IMesH_2)(C_5H_5N)_2(Cl)_2Ru{=}CHPh$ were synthesized according to published procedures.[1–3]

2. Synthesis and Purification of Peptide Monomers

Peptide Synthesis: Peptides were synthesized using a Liberty Blue (CEM) automated microwave peptide synthesizer, utilizing Fmoc-protected amino acids and standard solid-phase peptide synthesis (SPPS) protocols. All peptides were generated on Rink amide MBHA resin to give C-terminal amidated peptides. Peptide monomers used as comparisons to polymer samples, as well as for later polymerization, were capped with N-(hexanoic acid)-*cis*-5-norbornene-*exo*-2,3-dicarboxyimide using SPPS.

Cleavage from the resin was performed in 88:5:5:2 (% v/v) trifluoroacetic acid (TFA), water, phenol, and triisopropyl silane, respectively, for two hours. After filtration, the resin was washed three times with fresh trifluoroacetic acid and dichloromethane, before all fractions were concentrated using a rotary evaporator and precipitated in cold diethyl ether. The precipitated product was dried under vacuum to yield solid crude peptide that was purified as detailed below.

Analytical High-Performance Liquid Chromatography (HPLC): Analytical HPLC analysis of peptides was performed on a Jupiter 4μ Proteo 90Å Phenomenex column (150 x 4.60 mm) using a Hitachi-Elite LaChrom L-2130 pump equipped with UV-Vis detector (Hitachi-Elite LaChrom L2420). The solvent system consists of (A) 0.1% v/v TFA in water and (B) 0.1% v/v TFA in acetonitrile. After one column volume was monitored (3 mins), the solvent gradient was allowed to run (30 mins) before a wash step (not shown).

Preparative HPLC: A Gilson PLC 2050 purification system was used to purify all peptides. The solvent system consisted of (A) 0.1% TFA in water and (B) 0.1% TFA in acetonitrile. Samples were dissolved (<10 mg/mL), filtered through a 0.22 μM PES filter, and run using solvent gradients optimized by examination of analytical HPLC data. For the E-alpha, K-alpha, and A-alpha peptide monomers, the optimized gradient was 35 – 55% B, and for the random peptide monomer, the optimized gradient was 10 – 40% B.

Electrospray Ionization Mass Spectrometry (ESI-MS): ESI-MS spectra of peptides were collected using a Bruker amaZon SL mass spectrometer configured with an ESI source in both negative and positive ionization modes, using a mobile phase of 50% water and 50% acetonitrile.

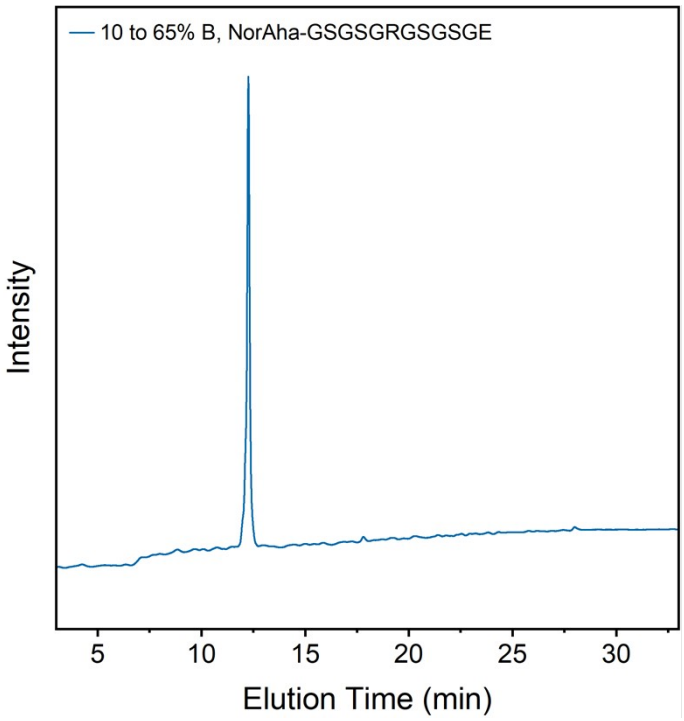

Figure S1. Analytical HPLC trace (obtained at 214 nm) of the random coil-based peptide monomer, NorAha-GSGSGRGSGSGE-NH_2, obtained after purification using preparative HPLC, using a solvent gradient of 10 to 65% B.

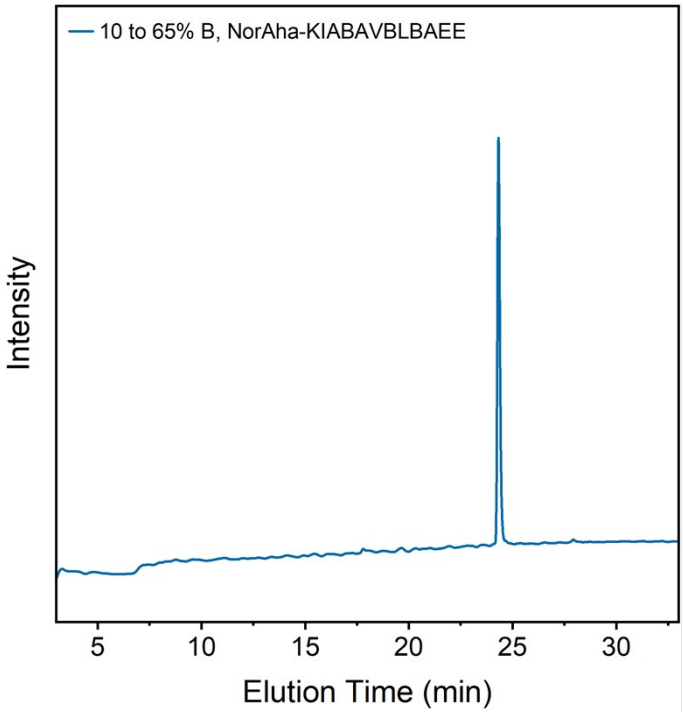

Figure S2. Analytical HPLC trace (obtained at 214 nm) of the alpha helix-based peptide monomer, NorAha-KIABAVBLBAEE-NH_2 ("E-alpha"), obtained after purification using preparative HPLC, using a solvent gradient of 10 to 65% B.

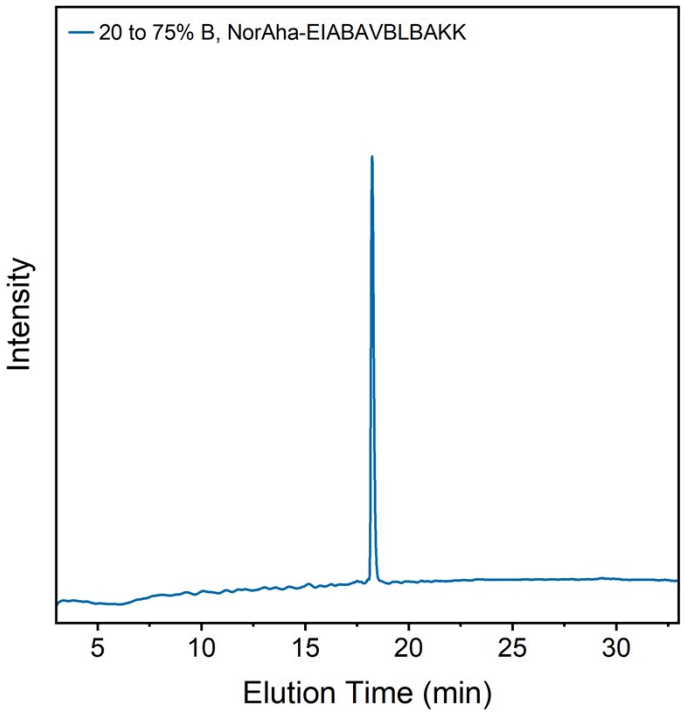

Figure S3. Analytical HPLC trace (obtained at 214 nm) of the alpha helix-based peptide monomer, NorAha-EIABAVBLBAKK-NH_2 ("K-alpha"), obtained after purification using preparative HPLC, using a solvent gradient of 20 to 75% B.

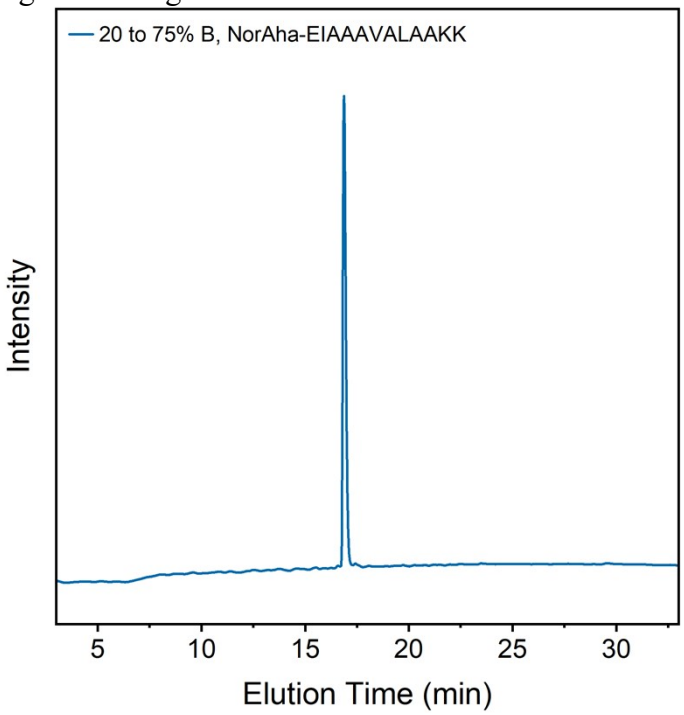

Figure S4. Analytical HPLC trace (obtained at 214 nm) of the alpha helix-based peptide monomer, NorAha-EIAAAVALAAKK-NH_2 ("A-alpha"), obtained after purification using preparative HPLC, using a solvent gradient of 20 to 75% B.

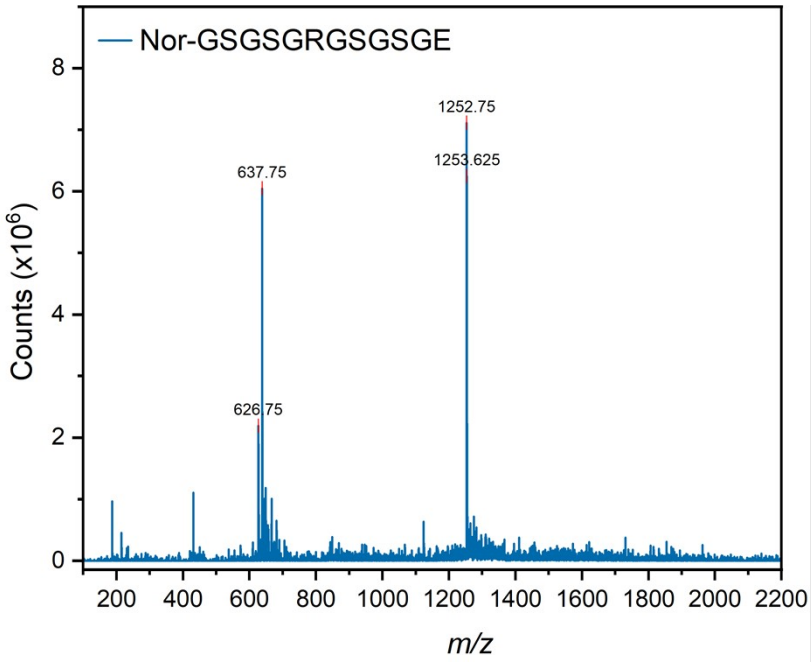

Figure S5. Plot of ESI-MS results of NorAha-GSGSGRGSGSGE-NH_2 after purification, confirming the successful synthesis and purification of the expected peptide. Expected *m/z* of [M+H] = 1252.56, [M+2H] = 626.78, [M+H+Na] = 637.77.

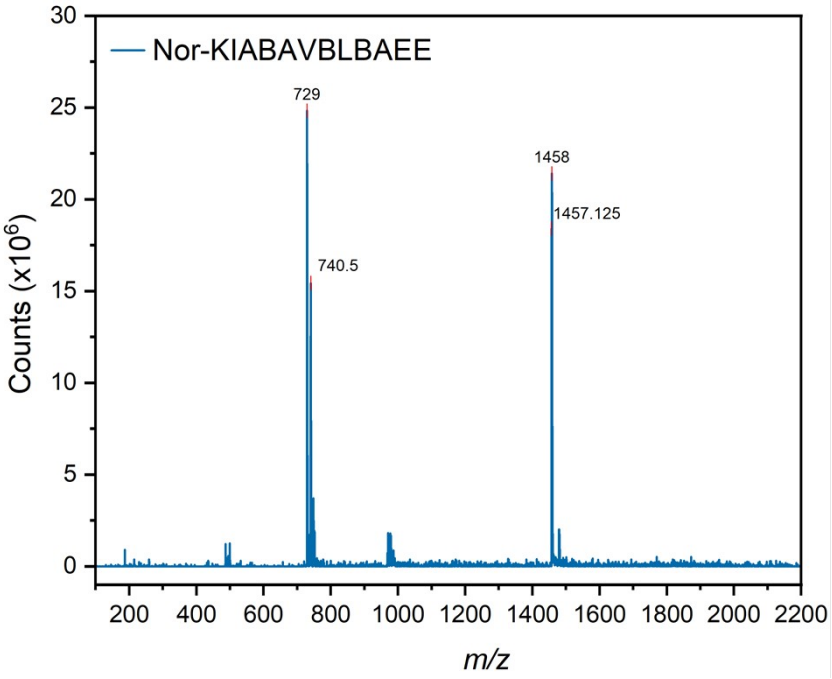

Figure S6. Plot of ESI-MS results of NorAha-KIABAVBLBAEE-NH_2 after purification, confirming the successful synthesis and purification of the expected peptide. Expected *m/z* of [M+H] = 1456.83, [M+2H] = 728.92, [M+H+Na] = 739.9.

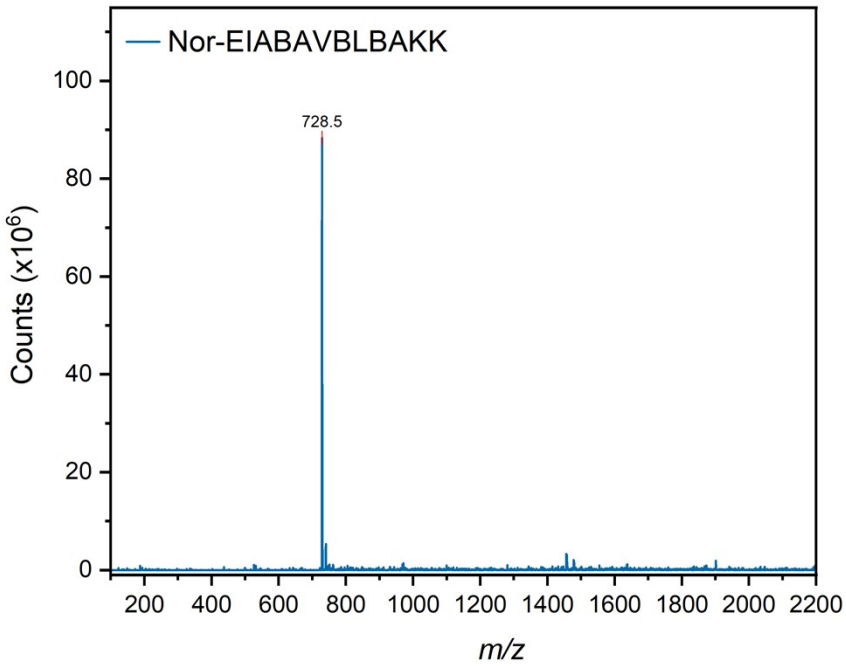

Figure S7. Plot of ESI-MS results of NorAha-EIABAVBLBAKK-NH_2 after purification, confirming the successful synthesis and purification of the expected peptide. Expected *m*/*z* of [M+H] = 1455.90, [M+2H] = 728.45.

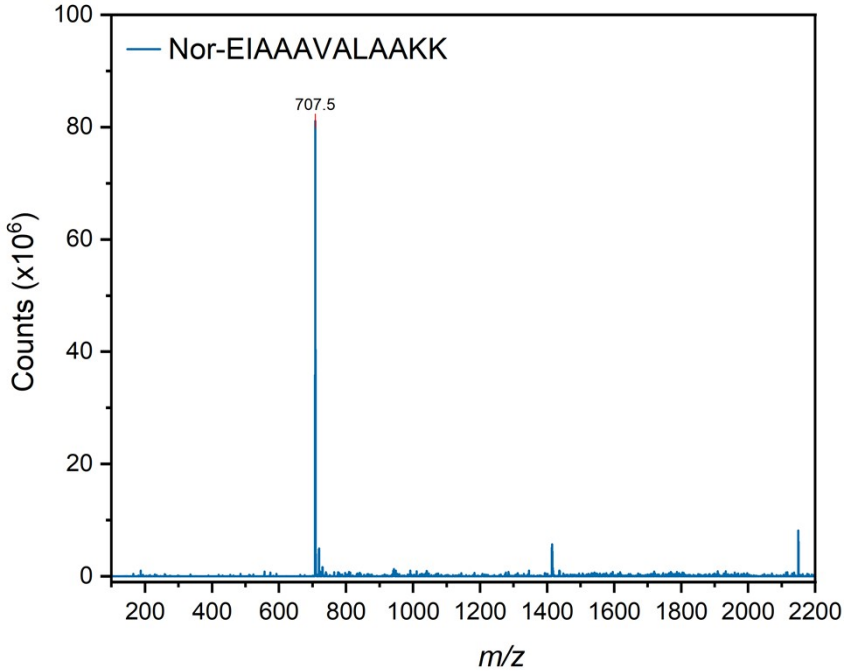

Figure S8. Plot of ESI-MS results of NorAha-EIAAAVALAAKK-NH_2 after purification, confirming the successful synthesis and purification of the expected peptide. Expected *m*/*z* of [M+H] = 1413.85, [M+2H] = 707.43.

3. Polymerization and Characterization of Polymers

Polymerization reactions were carried out in a purge box under a nitrogen atmosphere, similar to procedures previously described.[4,5] Solvent (*N,N*-dimethylformamide) was sparged with nitrogen gas immediately before use. Small-scale reactions were performed and monitored using ^{1}H NMR spectroscopy to assess the polymerization of the monomer before polymerizations with larger batches (>0.05 g) of peptide monomer were attempted. ^{1}H NMR spectra were measured on a Bruker Avance III spectrometer (400 MHz).

In a typical NMR-scale experiment, peptide monomer (15 to 45 mg) was dissolved in dry *N,N*-dimethylformamide (DMF, 0.5 mL) with or without lithium chloride (1 M; depending on solubility of polymer) and an internal standard (hexamethyldisilane, HMDS). The monomer solution was transferred to a J. Young NMR tube, sealed, and the NMR spectrum of the solution was measured. The integration of the norbornene alkene peak (6.3 ppm) was assessed relative to the integration of the hexamethyl peak (~0 ppm). Subsequently, the tube was brought into the purge box, a solution of Grubbs 3rd generation catalyst in DMF (1 eq.) was added, and the reaction was mixed. The NMR tube was sealed and then monitored regularly to observe the progress of the polymerization by observing the disappearance of the norbornene alkene peak. Typically, 60-150 min was required for complete conversion. The polymers were terminated with ethyl vinyl ether (>20 equiv) for 20 min at room temperature, precipitated, washed with cold diethyl ether 3 times, and collected by centrifugation.

The molecular weight and polydispersity of all polymers were determined by organic phase or aqueous phase gel permeation chromatography, or SDS-PAGE when polymers were found incompatible with gel permeation chromatography. For example, E-alpha and K-alpha-derived systems did not elute from the columns used for either aqueous or organic-phase GPC. We note that the SDS-PAGE values consistently underestimate the approximate molecular weight of polymer samples, likely due to the fact the polymer topology might hinder the binding of sodium dodecyl sulfate in comparison to a protein. This can be particularly discerned in the case of random$_{15}$, random$_{30}$, and random$_{45}$, where M_w values were obtained very close to the anticipated theoretical values via SEC-MALS, but MW values determined from SDS-PAGE significantly underestimate the weight of the polymer the longer the degree of polymerization (Table S1). We also note the underestimation of dispersity values determined using SEC-MALS, which is a limitation of this technique.[6]

Organic Phase Gel Permeation Chromatography (Organic GPC): Organic phase GPC measurements were performed on a set of Phenomenex Phenogel 5µ, 1K-75K, 300 x 7.80 mm in series with a Phenomex Phenogel 5µ, 10K-1000K, 300 x 7.80 mm columns with HPLC grade solvents as eluents: dimethylformamide (DMF) with 0.05 M of LiBr at 60 °C. Detection consisted of a Hitachi UV-Vis Detector L-2420, a Wyatt Optilab T-rEX refractive index detector operating at 658 nm and a Wyatt DAWN® HELEOS® II light scattering detector operating at 659 nm.

Aqueous Phase Gel Permeation Chromatography (Aqueous GPC): Aqueous phase GPC measurements were performed with a Tosoh Bioscience TSK-GEL®PWxl-CP column 7.8 mm ID x 30 cm, 10 µm, using either 0.1 M $NaNO_3$ with 0.1%TFA or 0.05% NaN_3 as the mobile phase. Detection consisted of a Wyatt Optilab T-rEX refractive index detector operating at 658 nm and a Wyatt DAWN® HELEOS® II light scattering detector operating at 659 nm.

Dynamic Light Scattering (DLS): DLS analyses were conducted at room temperature on a Zetasizer Nano-ZS (Malvern) operating with a 633 nm laser. Samples were prepared as 2.5 mg/mL solutions and measured at 25 ºC with an equilibration time of 60 seconds prior to measurement.

SDS-PAGE: Samples were dissolved to a concentration of 1 mg/mL in aqueous buffer or water, before being combined with Laemmli sample buffer (30 μL sample, 20 μL buffer solution; Bio-Rad) and were heated at 95 ºC for 10 minutes. The cooled samples were then loaded (20 μL) onto Mini-PROTEAN TGX Precast Protein Gel (Bio-Rad) with an acrylamide gel gradient of 4 to 15% and using a Tris/Gly/SDS running buffer (Bio-Rad). Molecular weight standards were utilized from Bio-Rad (Precision Plus Protein Dual Xtra). The gels were run at a voltage of 120 V for 1 hour at room temperature, after which the gels were stained with Coomassie Brilliant Blue G dye solution (containing 40% v/v methanol and 10% v/v acetic acid) for 1 hour. The gels were then destained (using solutions of 40% v/v methanol and 10% v/v acetic acid) until the gel background was clear while retaining stain in the sample and reference bands, then imaged using an Azure Biosystems Azure 600 Imaging System in the Keck Biophysics Facility at Northwestern University.

Table S1. A list of polymer samples that were generated and studied in the course of this study.

Polymer Sample	Theoretical M_n (kDa)	Experimental M_w (kDa)[a]	Experimental M_n (kDa)	$Đ$ (M_w/M_n)	MW (kDa)[b]	Aqueous R_h (nm, DLS)
E-alpha$_7$	10.2	–	–	–	11	2.4
E-alpha$_{15}$	21.9	–	–	–	18	2.2
E-alpha$_{30}$	43.7	–	–	–	37	3.2
E-alpha$_{45}$	65.6	–	–	–	50	3.1
E-alpha$_{90}$	131.1	–	–	–	120	7
K-alpha$_{15}$	21.8	24.7[c]	22.3[c]	1.11[c]	18	2.2
K-alpha$_{30}$	43.7	41.0[c]	39.8[c]	1.03[c]	30	2.1
K-alpha$_{45}$	65.5	59.0[c]	56.8[c]	1.04[c]	45	2.5
random$_{15}$	18.8	18.8[d]	18.6[d]	1.01[d]	20	3.2
random$_{30}$	37.6	40.7[d]	40.5[d]	1.01[d]	30	3.7
random$_{45}$	56.4	53.0[d]	51.5[d]	1.03[d]	50	3.9
random$_{90}$	112.7	–	–	–	95	3.6

[a] M_w and M_n values for PLPs derived from the E-alpha peptide sequence could not be determined as SDS-PAGE, the only method by which the molecular weight of the polymer sample could be measured, does not allow for the determination of these values.

[b] MW values determined by estimating the middle of the sample band via visual inspection of SDS-PAGE data (Figures S13-S14 and Fig. 2 in the main text).

[c] Measured using aqueous GPC in 0.05 % NaN_3 in water.

[d] Measured using aqueous GPC in 0.1 M $NaNO_3$ with 0.1% TFA.

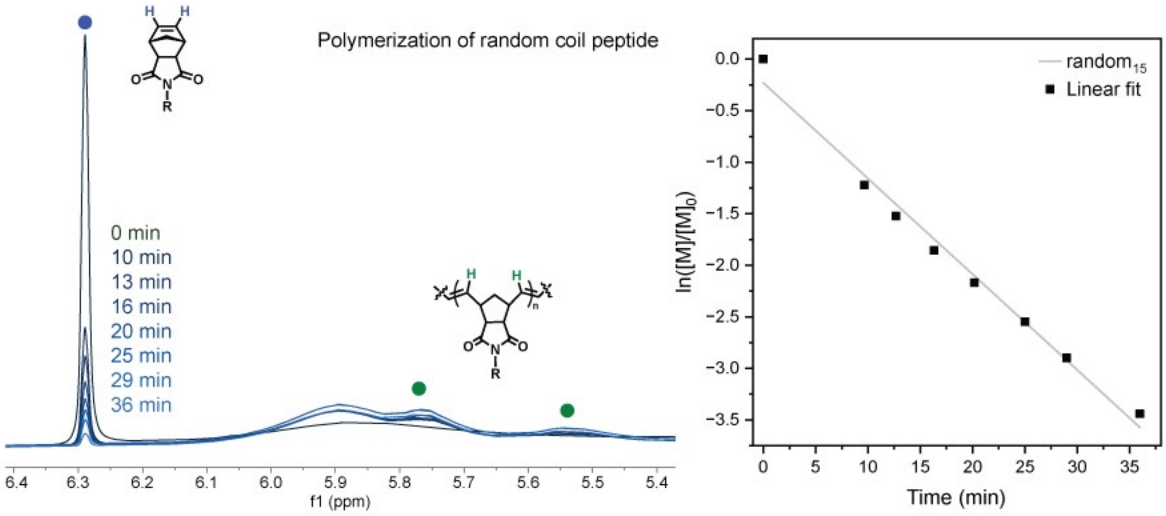

Figure S9. Representative polymerization of the random coil peptide monomer, NorAhaGSGSGRGSGSGE, using the Grubbs' third generation catalyst and targeting a 15-mer in length, monitored using ^{1}H NMR spectroscopy. Left: a close-up of the alkene region of the monomer (peak indicated with a blue circle) and polymer (broad peaks indicated with green circles). Right: pseudo-first-order kinetics plot of the polymerization, generated by integrating the monomer alkene peak relative to the integration of an HMDS standard peak. The plots were fit to a linear line with a slope of −0.0929 and R^2 = 98.6%.

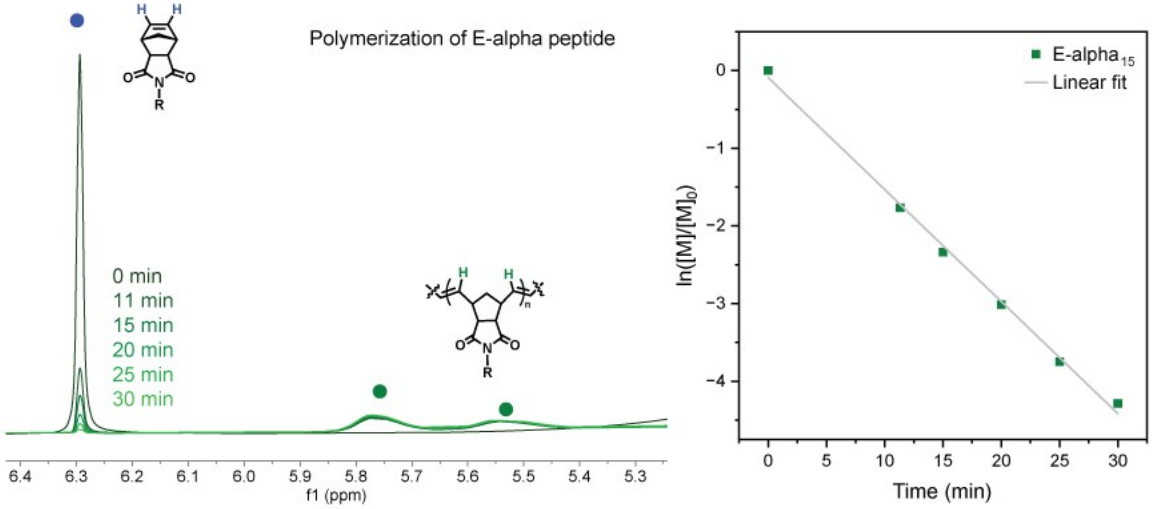

Figure S10. Representative polymerization of the E-alpha peptide monomer, NorAhaKIABAVBLAEE, using the Grubbs' third generation catalyst and targeting a 15-mer in length, monitored using ^{1}H NMR spectroscopy. Left: a close-up of the alkene region of the monomer (peak indicated with a blue circle) and polymer (broad peaks indicated with green circles). Right: pseudo-first-order kinetics plot of the polymerization, generated by integrating the monomer alkene peak relative to the integration of an HMDS standard peak. The plots were fit to a linear line with a slope of −0.1441 and R^2 = 99.7%.

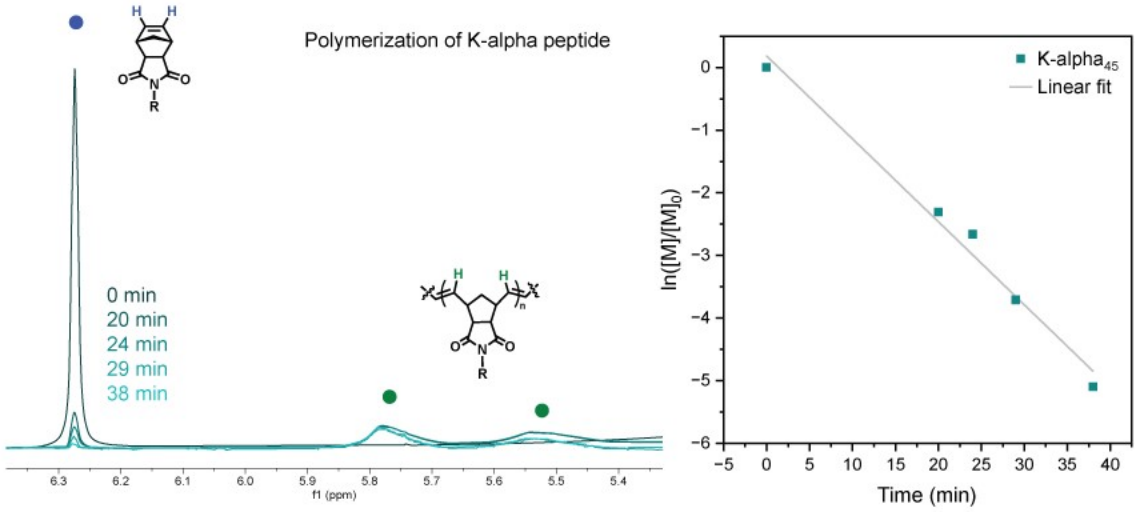

Figure S11. Representative polymerization of the K-alpha peptide monomer, NorAhaEIABAVBLAKK, using the Grubbs' third generation catalyst and targeting a 45-mer in length, monitored using ^{1}H NMR spectroscopy. Left: a close-up of the alkene region of the monomer (peak indicated with a blue circle) and polymer (broad peaks indicated with green circles). Right: pseudo-first-order kinetics plot of the polymerization, generated by integrating the monomer alkene peak relative to the integration of an HMDS standard peak. The plots were fit to a linear line with a slope of −0.1324 and R^2 = 97.8%.

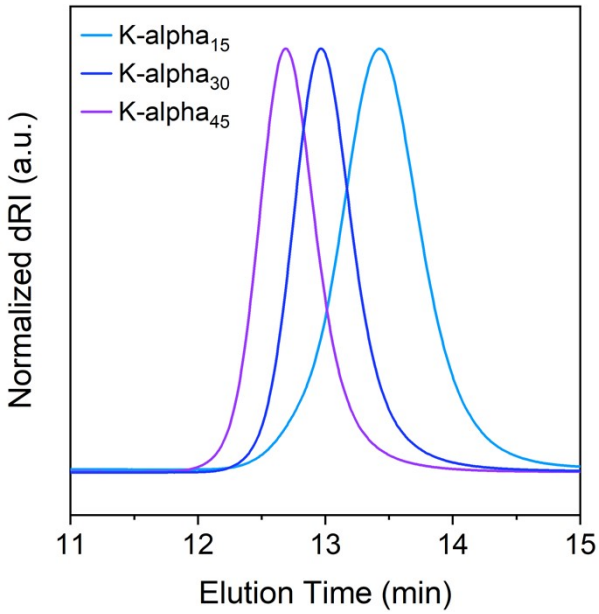

Figure S12. Aqueous SEC-MALS of the K-alpha polymers, K-alpha$_{15}$ (light blue trace), K-alpha$_{30}$ (blue trace), and K-alpha$_{45}$ (purple trace), run using 0.05 wt% NaN_3 in water. The differential refractive index was normalized to the highest and lowest values of the run's data to allow for a more facile comparison.

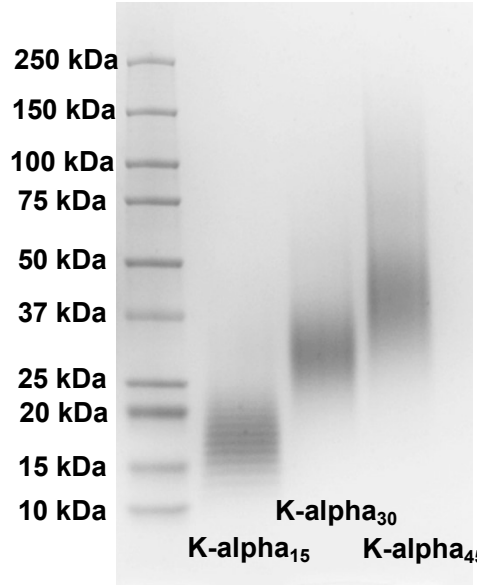

Figure S13. SDS-PAGE gel of α-helical peptide-brush polymers based on the K-alpha peptide monomer. Approximate average molecular weight was estimated from analysis of the band positions relative to the positions of the molecular weight ladders (far left).

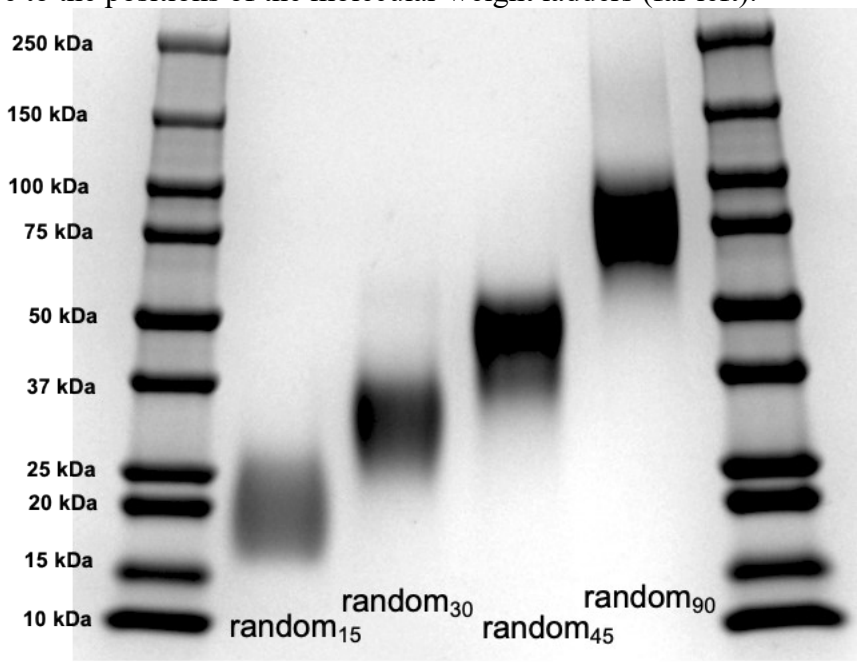

Figure S14. SDS-PAGE gel of random coil peptide-brush polymers. Approximate average molecular weight were estimated from analysis of the band positions relative to the positions of the molecular weight ladders (far left and right).

4. Circular Dichroism Spectroscopy

Circular dichroism (CD) spectra were obtained on a JASCO J-815 spectrometer equipped with a Peltier sample holder for temperature control in the Keck Biophysics Facility at Northwestern University. Samples were dissolved in various solvents (e.g. 50 mM sodium acetate buffer pH 4;

50 mM sodium carbonate buffer at pH 10; 50% methanol with water or buffered solution; and 100% methanol with 3 μM NaOH or TFA depending on the solubility of the peptide or polymer). These solutions were approximately 100 μM with respect to peptide monomer concentration, and placed into a 0.1 mm quartz cuvette (Hellma). Measurements were obtained using a scan speed of 10 nm/min, using a 1 nm bandwidth, 4 sec response time, and with three accumulations. Background spectra of solvent were obtained prior to measurement of the sample solutions and subtracted from the sample spectra using JASCO Spectra Analysis. Spectra were not smoothed.

For temperature scans, sample temperature was varied between 20 and 92 ºC with steps of 1 ºC/min while monitoring ellipticity at 222 nm. At all endpoints of the temperature ramps (20 and 92 ºC), full CD spectra were obtained.

To estimate secondary structure content, two approaches were employed. First, the values were analyzed by examining the intensity of the spectrum at 222 nm, which is highly sensitive to the degree of helicity present. The value for a completely unfolded peptide was estimated from the value of the A-alpha monomer in water at 222 nm (−3,850 deg•cm^2/dmol), and a completely folded system was estimated from the value of the E-alpha monomer in 100% methanol (−8,390 deg•cm^2/dmol after the unfolded correction). The values at 222 nm for all samples were corrected for the background signal from the unfolded system and then compared to the value for a completely folded system. Secondly, the spectra were analyzed using the CDPro program implemented in the JASCO Spectra Manager software, using the CONTIN algorithm and SMP56 reference set,[7] and assuming concentration of 0.0013 dmol/L. These values showed excellent agreement with the experimentally-determined percentages (Table S2 and S3).

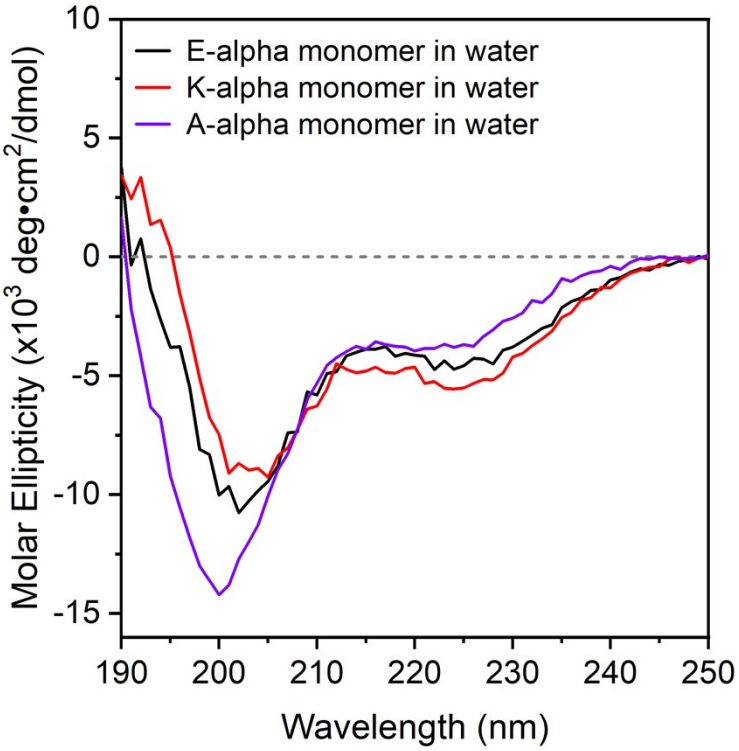

Figure S15. CD spectra of the peptide monomers E-alpha (black trace), K-alpha (red trace), and A-alpha (purple trace), measured at 25 ºC in aqueous buffer. Specifically, E-alpha was measured

in 50 mM sodium carbonate buffer (pH 10), and the samples K-alpha and A-alpha were measured in 50 mM sodium acetate buffer (pH 4).

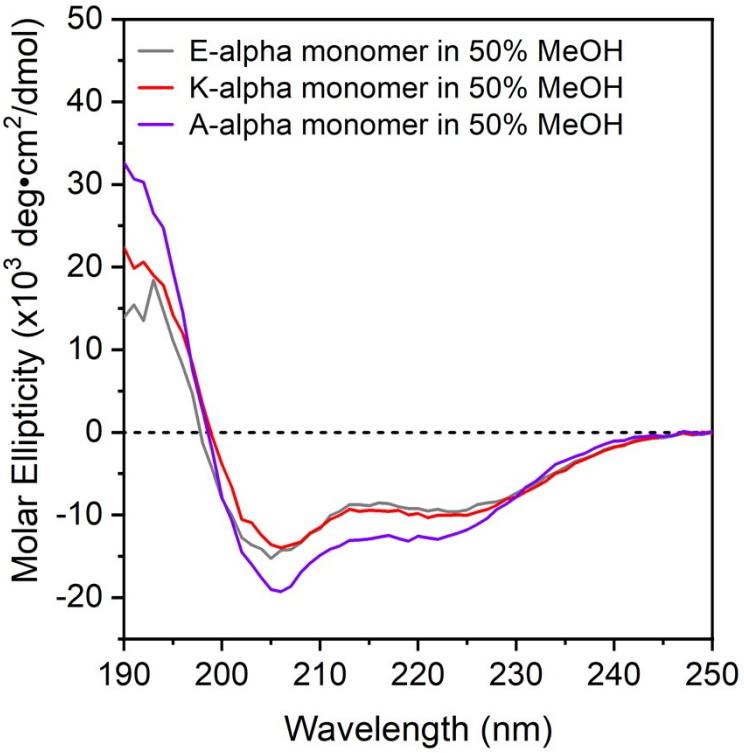

Figure S16. CD spectra of the peptide monomers E-alpha (black trace), K-alpha (red trace), and A-alpha (purple trace), measured at 25 ºC in 50% methanol. Specifically, E-alpha was measured in 50% methanol with 50 mM sodium carbonate buffer, and the samples K-alpha and A-alpha were measured in 50% methanol with 50 mM sodium acetate buffer.

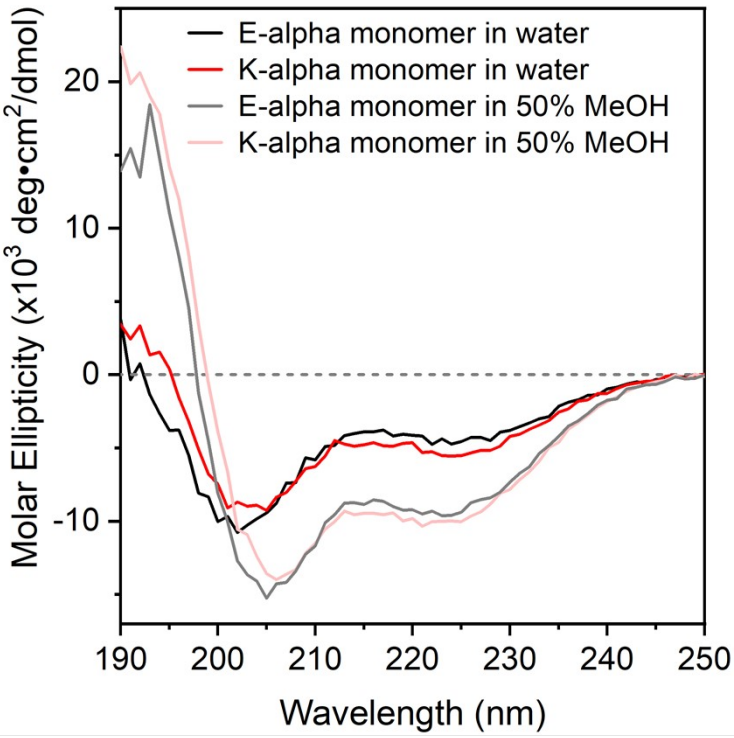

Figure S17. CD spectra of E-alpha monomer (black trace) and K-alpha monomer (red trace) in aqueous buffer, and E-alpha monomer (gray trace) and K-alpha monomer (pink trace) in 50% methanol, measured at 25 ºC. Specifically, E-alpha was measured in 50 mM sodium carbonate buffer or 50% methanol with 50 mM sodium carbonate buffer, and K-alpha was measured in 50 mM sodium acetate buffer or 50% methanol with 50 mM sodium acetate buffer.

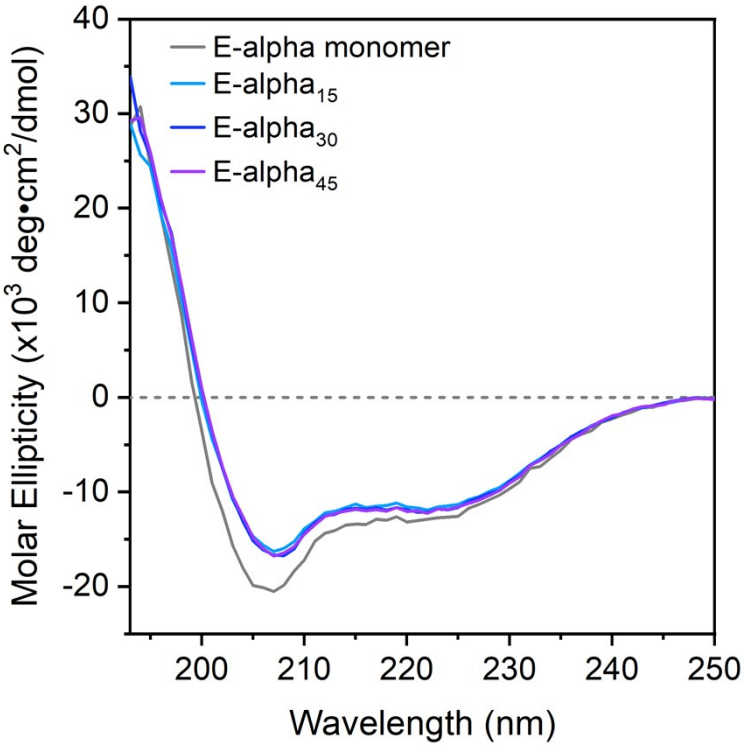

Figure S18. CD spectra of E-alpha-derived peptide monomer and polymers measured at 25 ºC and in 100% MeOH with 3 mM NaOH. Monomer, 15-mer, 30-mer, and 45-mer polymers were represented by gray, azure, dark blue, and purple traces respectively.

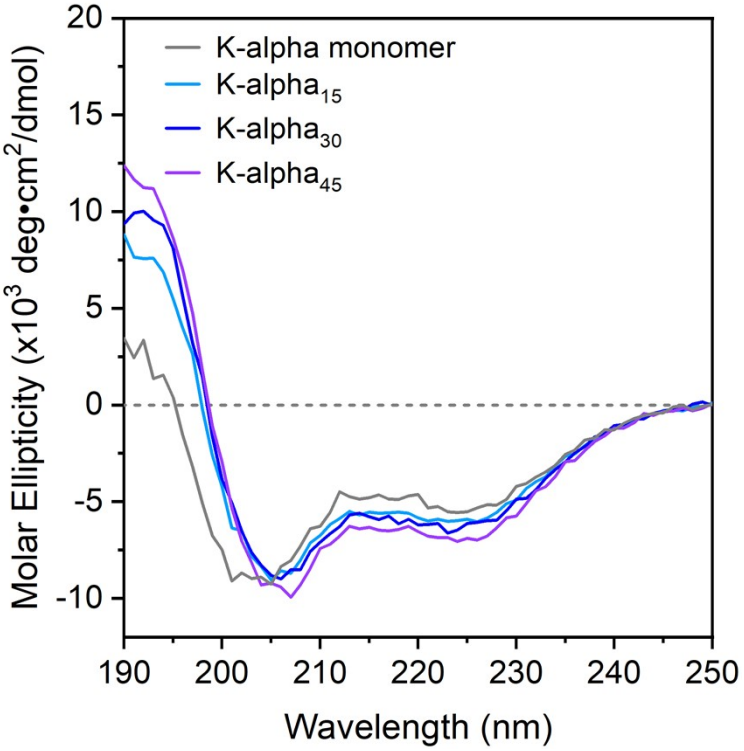

Figure S19. CD spectra of K-alpha-derived peptide monomer and polymers measured at 25 ºC and in 50 mM sodium acetate buffer (pH 4). Monomer, 15-mer, 30-mer, and 45-mer polymers were represented by gray, azure, dark blue, and purple traces respectively.

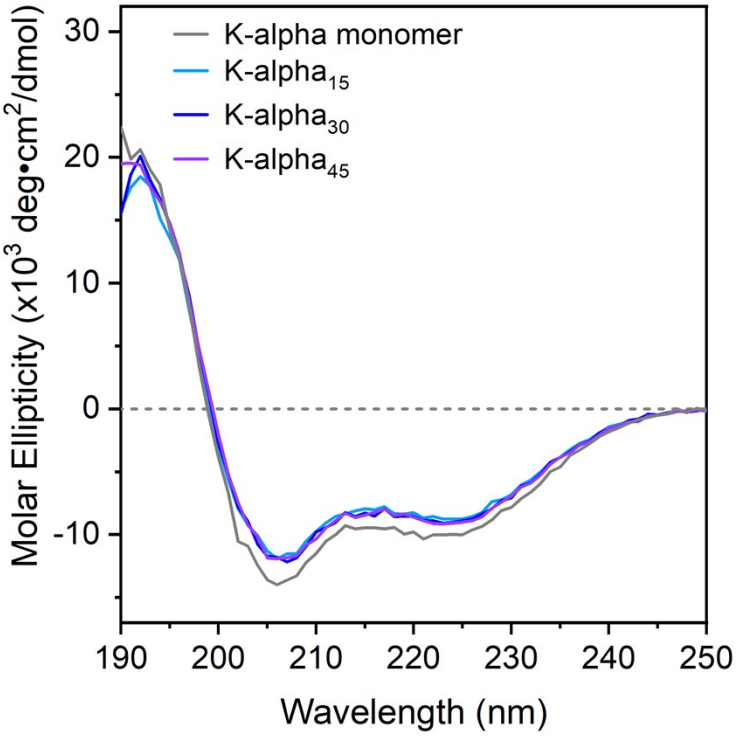

Figure S20. CD spectra of K-alpha-derived peptide monomer and polymers measured at 25 ºC and in 50 mM sodium acetate buffer (pH 4). Monomer, 15-mer, 30-mer, and 45-mer polymers were represented by gray, azure, dark blue, and purple traces respectively.

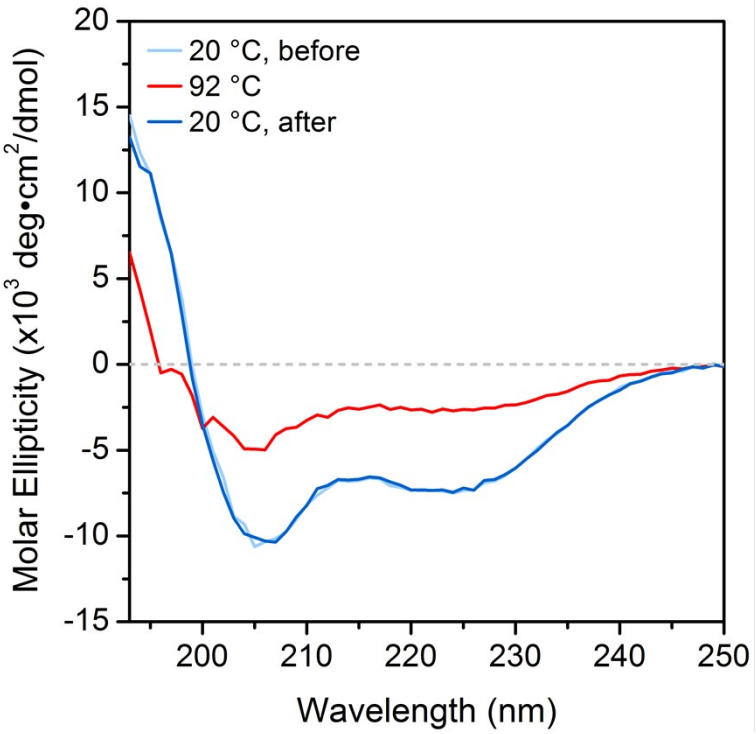

Figure S21. CD spectra of E-alpha$_{45}$ at 20 ºC (light blue trace), then after slowly (1 ºC/min) heating to 92 ºC (red trace), then after cooling slowly (1 ºC/min) back down to 20 ºC (blue trace).

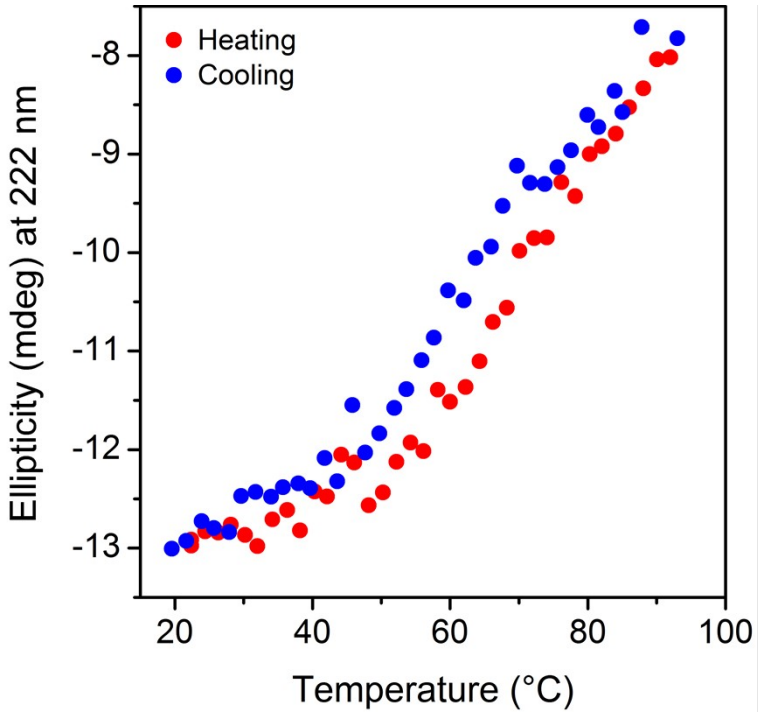

Figure S22. Ellipiticity of E-alpha$_{45}$ monitored at 222 nm during heating to 92 ºC at 1 ºC/min (red dots), and then while cooling to 20 ºC at 1 ºC/min (blue spheres).

Table S2. A list of polymer samples that were synthesized and studied in the course of this study, as well as their CD spectrum intensity at 222 nm, subtracted as described above, and the corresponding % folded.

Number of Repeats	Intensity at 222 nm (subtracted)	% Folded as Helical
E-alpha monomer	0.9	10.7%
E-alpha$_7$	0.43	5.1%
E-alpha$_{15}$	1.98	23.6%
E-alpha$_{30}$	2.9	34.6%
E-alpha$_{45}$	3.63	43.3%
E-alpha$_{90}$	3.87	46.1%

Table S3. Secondary structure content values from CDPro fitting, using CONTIN algorithm and SMP56 reference set.

Number of Repeats	% Folded as Helix (total)	% Folded as Beta Sheet (total)	% Folded as Turn	% Folded as Random
E-alpha monomer	10	32.9	23.1	33.8
E-alpha$_7$	14.2	35.8	21.1	28.9
E-alpha$_{15}$	23.4	23.3	22.4	30.8
E-alpha$_{30}$	35.6	15.4	21.6	27.4
E-alpha$_{45}$	34.3	17.1	21.4	27.2

5. Well-tempered Metadynamics Molecular Dynamics (MD) Simulations

The folding behavior of proteins and peptides is known to be slow. As such, advanced sampling of metadynamics simulations was carried out to quantify the probability of the α-helix secondary structure of peptides. Here the NorAhaKIABAVBLBAEE peptide-based macromonomer (E-alpha) was simulated. The metadynamics simulations were conducted using GROMACS 2023.0[8] with the patched Plumed 2.9.0.[9]

In metadynamics simulations, a history-dependent Gaussian bias potential is added to the Hamiltonian of the system as a function of collective variables (CVs).[10] The added Gaussian bias potential fills the underlying free energy basins and reflects the free energy surface (FES) as a function of the CVs. In well-tempered metadynamics, the height of the Gaussian bias potential continuously decreases over simulation time to ensure the convergence of the final bias potential to the actual FES.[11]

In this work, the collective variable of alphaRMSD[12] was employed. alphaRMSD calculates the RMSD of a segment of six connecting amino acids and computes the distance with a reference α-helical structure. It measures the number of segments that take the α-helix configuration using the following equation.

$$s = \sum_i \frac{1 - \left(\frac{r_i - d_0}{r_0}\right)^n}{1 - \left(\frac{r_i - d_0}{r_0}\right)^m}$$

The default values of n = 8, m = 12, d_0 = 0 and r_0 = 0.08 nm were employed.[12] The calculated numbers of α-helix configurations were normalized by the maximum allowed number of α-helix configurations in the peptide to calculate the probability of α-helix configurations. The maximum number of α-helix configurations is 7 for peptide KIABAVBLBAEE given that a segment of six connecting amino acids can form an α-helix structure.

The macromonomer was dissolved in a water box of around 6 nm in all dimensions. A salt concentration of 0.14 M NaCl was used. The CHARMM 36m potential[13] was employed along with the CGenFF parameters of the macromonomer backbone we recently developed.[5] CHARMM 36m was improved from an earlier version of CHARMM 36 to better describe unstructured proteins/peptides. The recommended CHARMM TIP3P[14] water model was utilized with the water structures constrained via the SETTLE algorithm.[15]

The system was first equilibrated using the steepest descent algorithm. It was further equilibrated for a duration of 1 ps using the canonical ensemble (constant number of particles, volume, and temperature, NVT) and a duration of 10 ps using the isothermal-isobaric ensemble (constant number of particles, pressure, and temperature, NPT). The system was eventually equilibrated for another 20 ns. The periodic boundary conditions were applied in all three dimensions. The neighbor searching was calculated up to 12 Å using the Verlet particle-based method and updated every 20-time steps. The short-range electrostatic interactions were truncated at the cut-off distance of 12 Å and the Smooth Particle Mesh Ewald (PME) algorithm[16,17] was applied for the long-range interactions. The Lennard-Jones 12-6 interactions were switched off from 10 to 12 Å via the potential-switch method in GROMACS. The NPT ensemble was used. The temperatures of water molecules and others were separately coupled using the Nosé-Hover algorithm (reference temperature 298 K, characteristic time 1 ps). The isotropic Parrinello-Rahman barostat was applied

with the reference pressure of 1 bar, the characteristic time was 4 ps, and the compressibility of 4.5×10^{-5} bar^{-1}. All the hydrogen-involved covalent bonds were constrained, which supported an integration time step of 2 fs. These parameters were recommended for the accurate reproduction of the original CHARMM simulation on lipid membranes[18] and have been verified in our simulations on peptide-brush polymers,[5,19] proteins,[20] polymers,[21] and lipid membranes.[22]

For the well-tempered metadynamics, the Gaussian bias potential was deposited every 1 ps with the initial height of 5 kJ/mol and a bias factor of 10. The temperature of the system was 298.15 K. The Gaussian width (sigma) is 1. The well-tempered metadynamics run for a duration of 5 μs. The convergence is provided in Fig. S23. The calculated free energy surface (FES) is provided in Fig. S24, along with the characteristic structures of the global minimum energy and local minimum energy structures.

To examine the distributions of the α-helix and other kinds of secondary structures on the peptide chain, we also carried out nonbiased MD simulations on the same system. Five parallel simulations were conducted, each for a simulation duration of 4 μs (a total of 20 μs). We then analyzed the secondary structures for individual amino acids. The calculated probabilities for all amino acids are presented in Fig. S25.

In addition to the macromonomer system, we also examined the corresponding polymer with DP = 15 using nonbiased MD and well-tempered metadynamics simulation. For the nonbiased MD simulations, five parallel simulations were conducted, each for a duration of 4 μs (a total of 20 μs). The radius of gyration of the polymer was calculated to be 1.94 ± 0.08 nm where the uncertainty stood for the standard deviation. The small fluctuation supports an approximately globular morphology of the polymer chain, which is consistent with the SAXS calculation presented in the main text (Fig. 7). For the well-tempered metadynamics simulations, they, unfortunately, did not converge in terms of the probability of α-helix for all the side chains of peptides after around 3 million CPU core hours on the supercomputer Frontera at the *Texas Advanced Computing Center* (TACC). It was thus not presented here. The slow convergence was likely owing to the large number (15) of peptide chains, each with 12 amino acids.

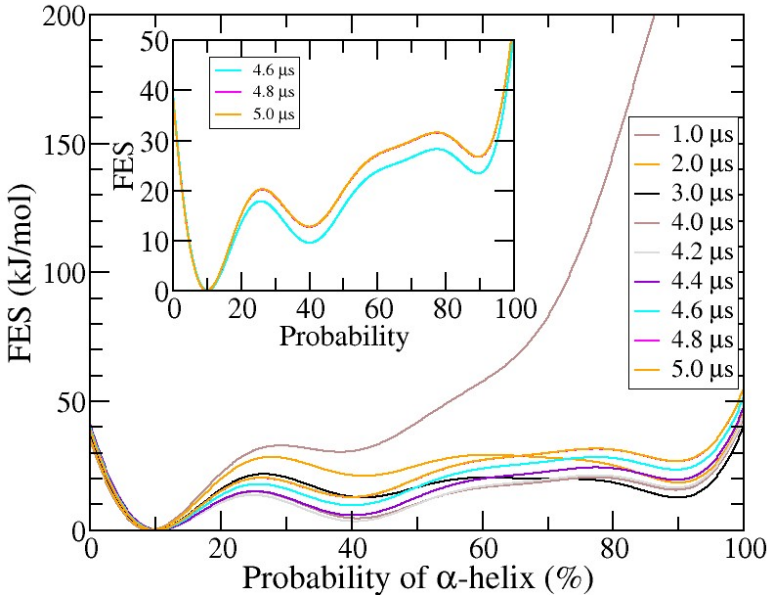

Figure S23. Convergence of the well-tempered metadynamics. The whole free energy surface (FES) profile is converged at 4.8 μs, with the location of global minimum converged at less than 1 μs.

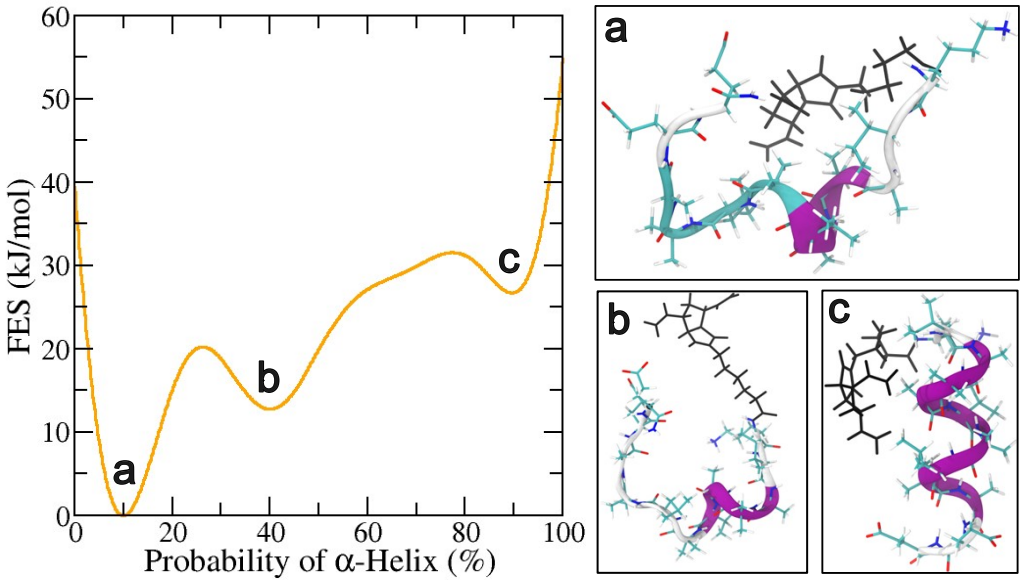

Figure S24. Free energy surface as a function of the probability of α-helix for KIABAVBLBAEE-based macromonomers obtained from well-tempered metadynamics simulations. A probability of 10% is the most energetically stable with a characteristic structure provided in inset (a). The α-helix/turn/random coil secondary structures of the peptide backbone are colored in magenta/cyan/white, respectively. The NorAha backbone atoms are colored in black with carbon/oxygen/hydrogen atoms colored in cyan/red/white, respectively. Demonstrated in insets (b) and (c) are the local minimum energy structures.

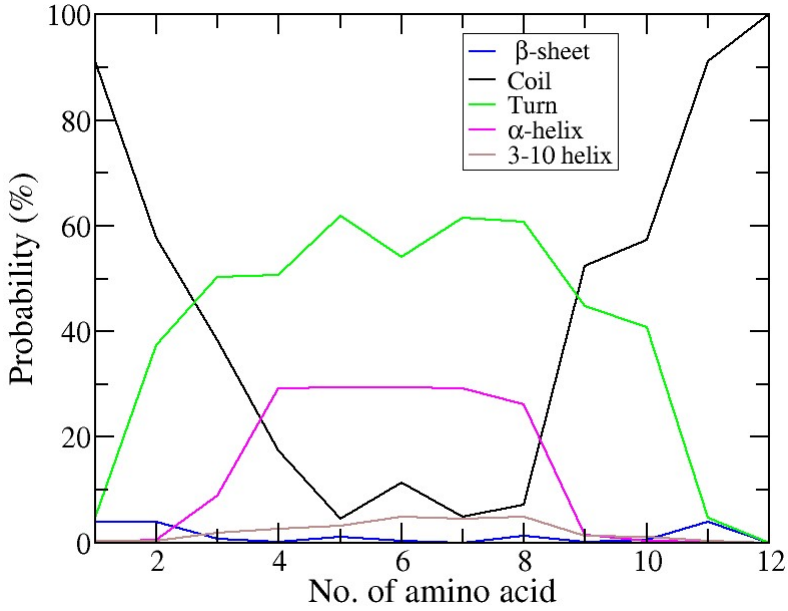

Figure S25. Distribution of the secondary structures on the KIABAVBLBAEE peptide of the macromonomer. Data are from five parallel nonbiased atomistic simulations, each with a simulation duration of 4 μs (a total of 20 μs).

6. Nuclear Magnetic Resonance Spectroscopy

1D and 2D NMR spectra with solvent suppression were recorded on a 600 MHz Bruker NEO spectrometer equipped with a QCI-F cryoprobe in the Northwestern University IMSERC facility. Purified peptide monomer or polymer samples were dissolved in the appropriate solvent, either 100 mM sodium carbonate buffer (pH 10) prepared with 90% H_2O and 10% D_2O, 100 mM sodium acetate (NaOAc-d_3) buffer (pH 4) prepared with 90% H_2O and 10% D_2O, or 100% CD_3OH. Peptide monomer samples were approximately 10 mM, and polymer samples were approximately 5 mM with respect to peptide monomer concentration. Generally, the 2D TOCSY spectra were measured using the dipsi2esgpph pulse sequence, using 8 scans, a scan width of 11.9 ppm, and 512 increments. 2D NOESY spectra were measured with the noesyesgpph pulse sequence, using 8 scans, a scan width of 11.9 ppm, 512 increments, and a d1 time of 1.5 s.

For H/D exchange experiments specifically, samples were dissolved in completely deuterated solvent (D_2O or CD_3OD), at which point their 1H NMR spectra were monitored periodically for one hour. All spectra except the K-alpha monomer in D_2O were obtained on a Bruker NEO 600 MHz spectrometer equipped with a cryoprobe; the K-alpha monomer in D_2O was measured on a Bruker Avance 600 MHz spectrometer.

All spectra were processed, viewed, and assigned using MestReNova, including the TOCSY and NOESY peaks.[23]

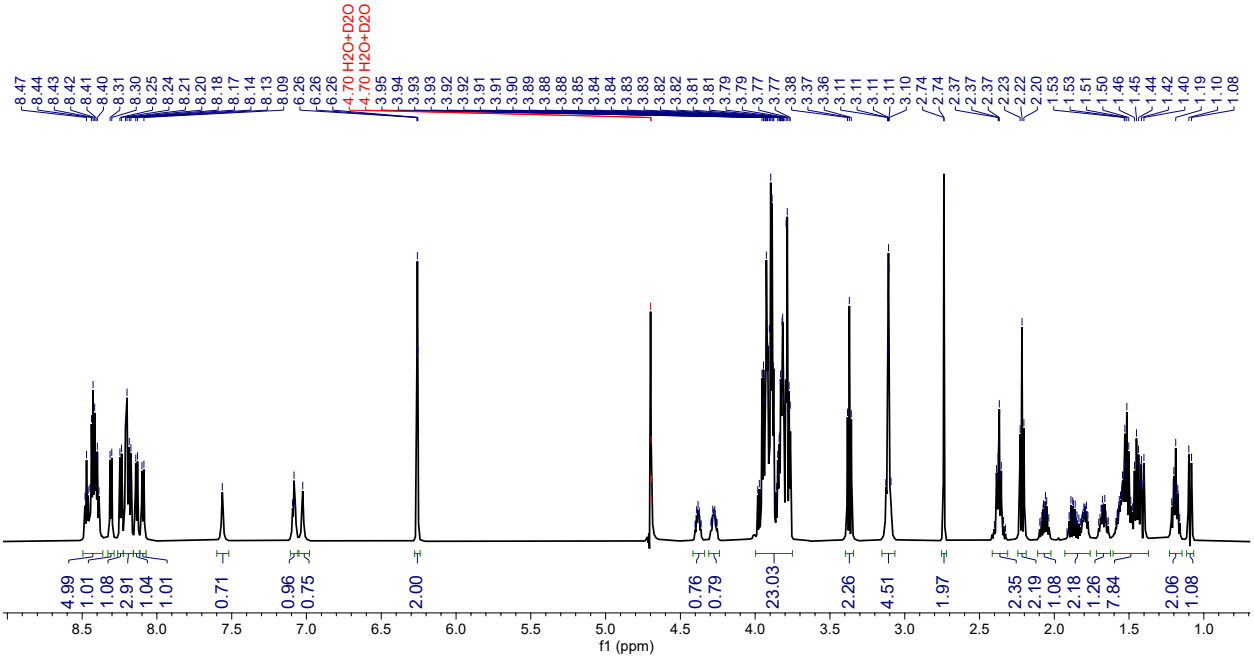

Figure S26. ^{1}H NMR spectrum of the random peptide monomer in 90% H_2O and 10% D_2O (approximately 10 mM), with solvent suppression, which was obtained on a 600 MHz spectrometer at 25 ºC.

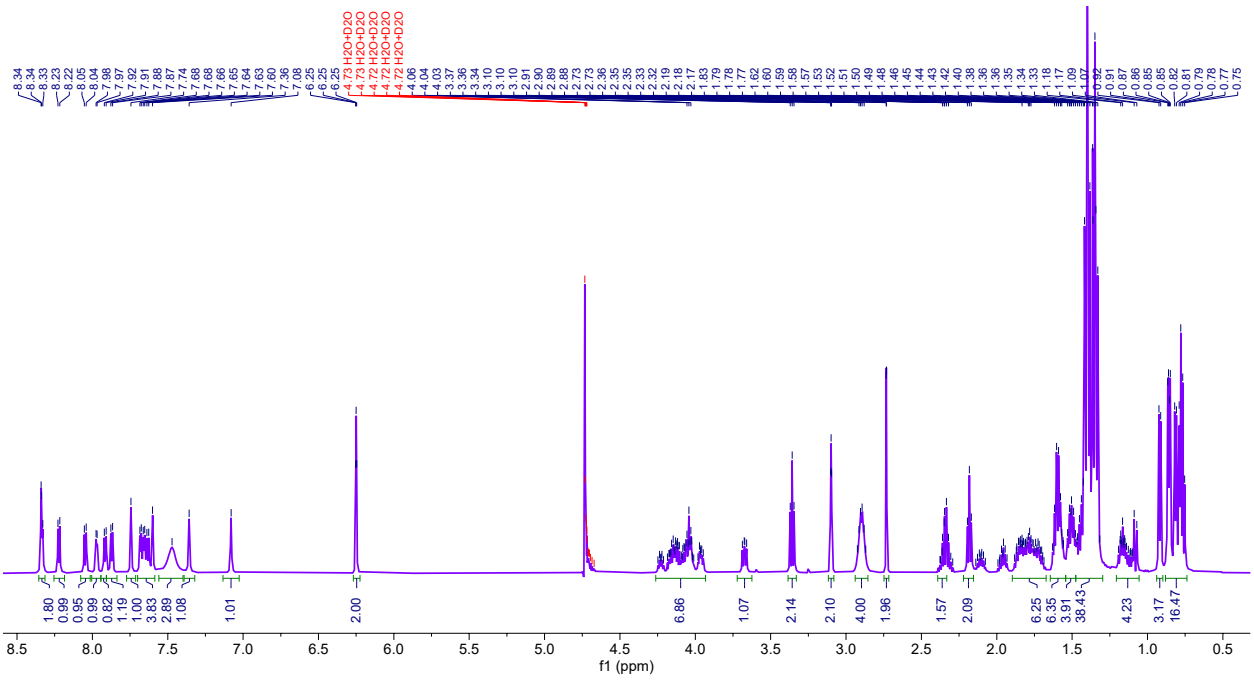

Figure S27. ^{1}H NMR spectrum of the K-alpha peptide monomer in 90% H_2O, 10% D_2O (100 mM NaOAc-d_3 buffer, approximately 10 mM peptide concentration), with solvent suppression, which was obtained on a 600 MHz spectrometer at 25 ºC.

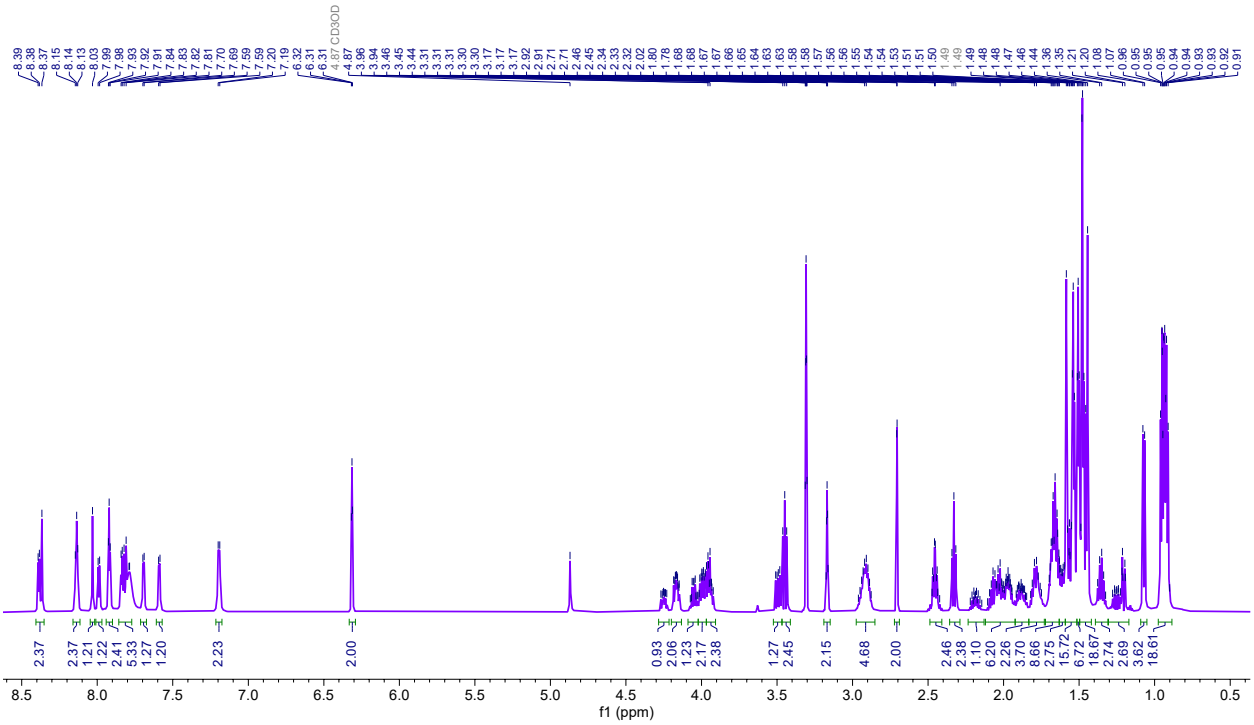

Figure S28. ^{1}H NMR spectrum of the K-alpha peptide monomer in CD_3OH (approximately 10 mM), with solvent suppression, which was obtained on a 600 MHz spectrometer at 25 ºC.

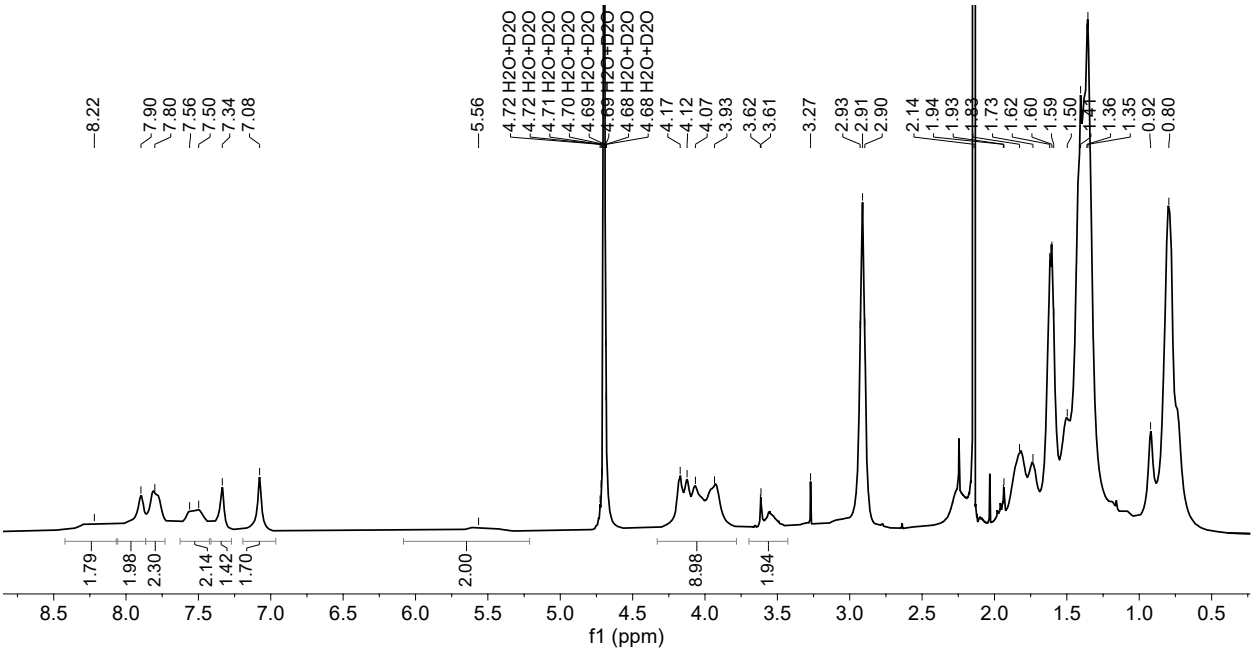

Figure S29. ^{1}H NMR spectrum of K-alpha$_{15}$ in H_2O/D_2O (approximately 5 mM with respect to peptide monomer concentration), with solvent suppression, which was obtained on a 600 MHz spectrometer at 25 ºC.

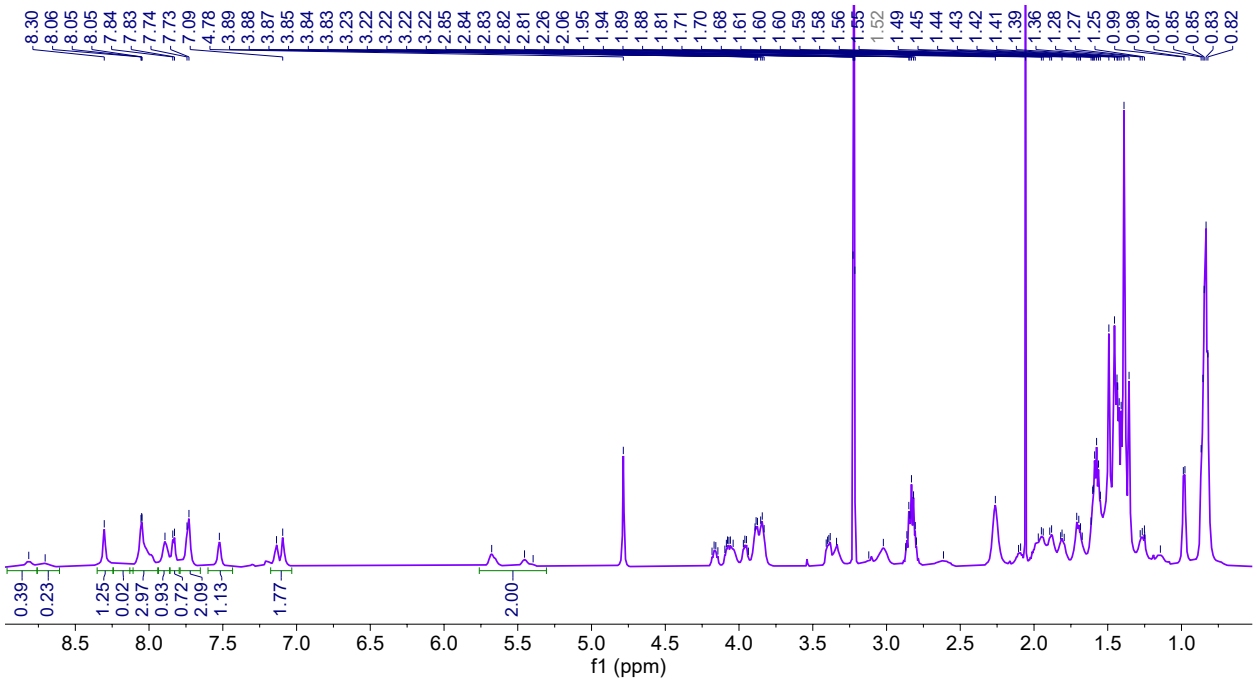

Figure S30. ^{1}H NMR spectrum of K-alpha$_{15}$ in CD_3OH (approximately 5 mM with respect to peptide monomer concentration), with solvent suppression, which was obtained on a 600 MHz spectrometer at 25 ºC.

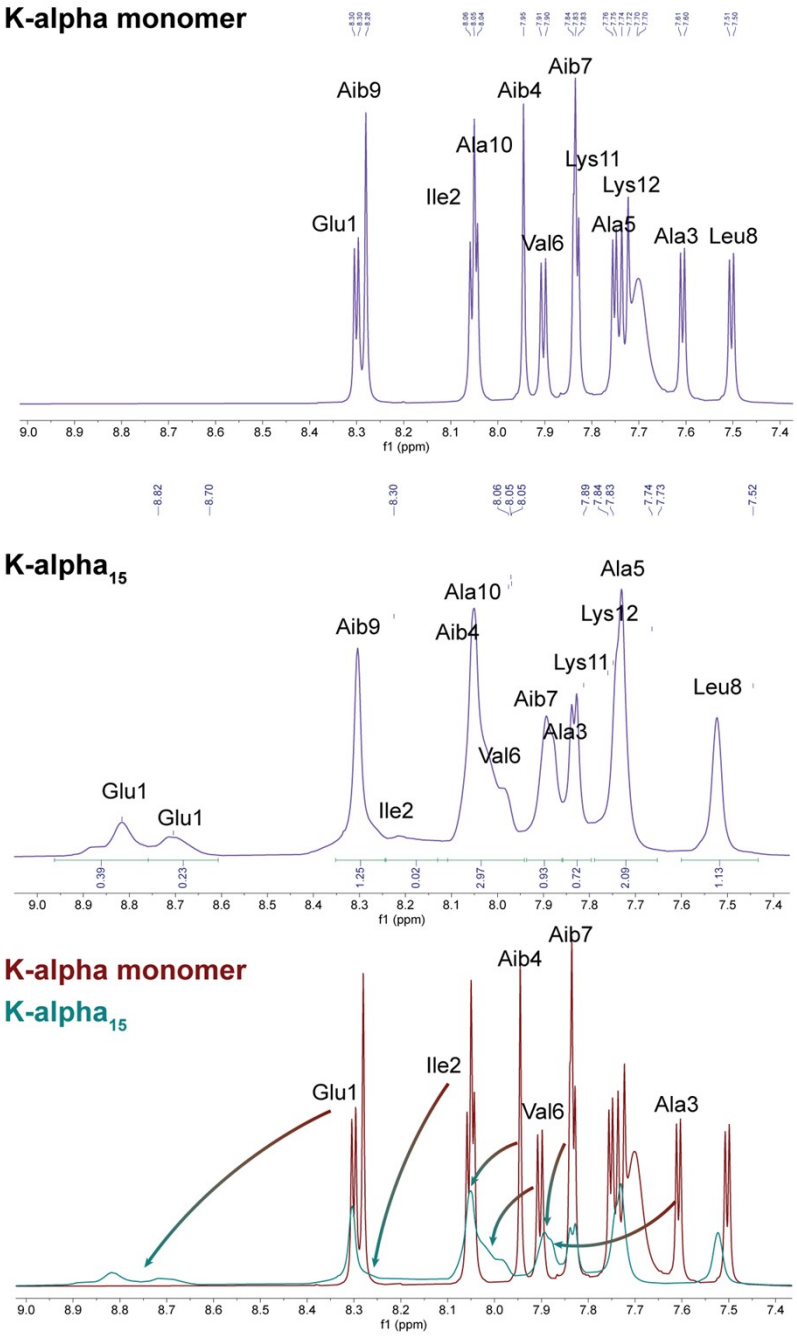

Figure S31. ^{1}H NMR spectra of the K-alpha peptide monomer and K-alpha$_{15}$ polymer in CD_3OH (approximately 10 mM and 5 mM with respect to peptide monomer concentration respectively), with solvent suppression, obtained on a 600 MHz spectrometer at 25 ºC. The top two panels demonstrate the ^{1}H NMR spectra of the respective sample, and the bottom panel overlays the two spectra and demonstrates with arrows how several key amino acids change position from the monomer (maroon trace) to the 15-mer (turquoise trace). The most dramatic shifts appear with residues near the N-terminus, consistent with their proximity to the polymer backbone.

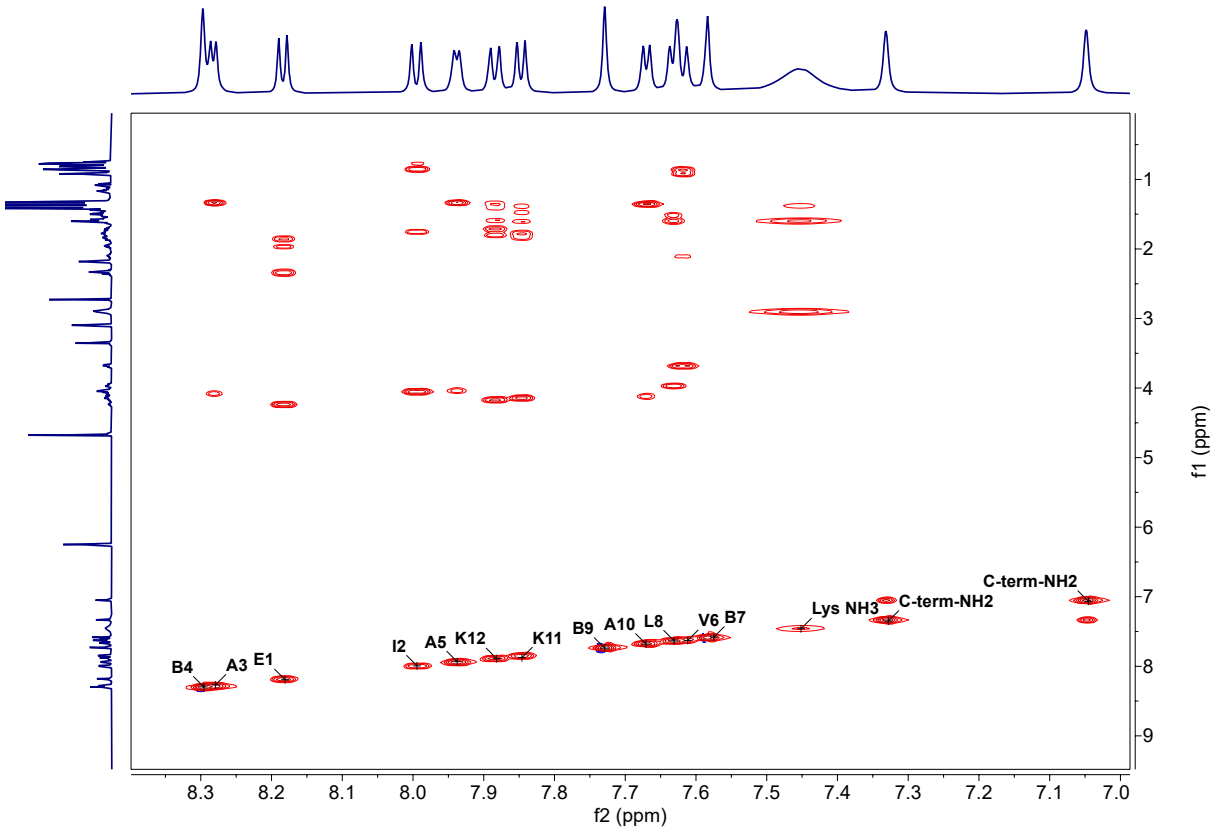

Figure S32. 2D TOCSY spectrum of the K-alpha monomer in 90% H_2O, 10% D_2O (approximately 10 mM), with solvent suppression, obtained on a 600 MHz spectrometer at 25 ºC. Labels indicate the amino acid residue of the corresponding amide NH peak. The figure highlights in particular the diagonal peaks in the NH amide region and cross-peaks of these NH peaks with the αH and side chain moieties.

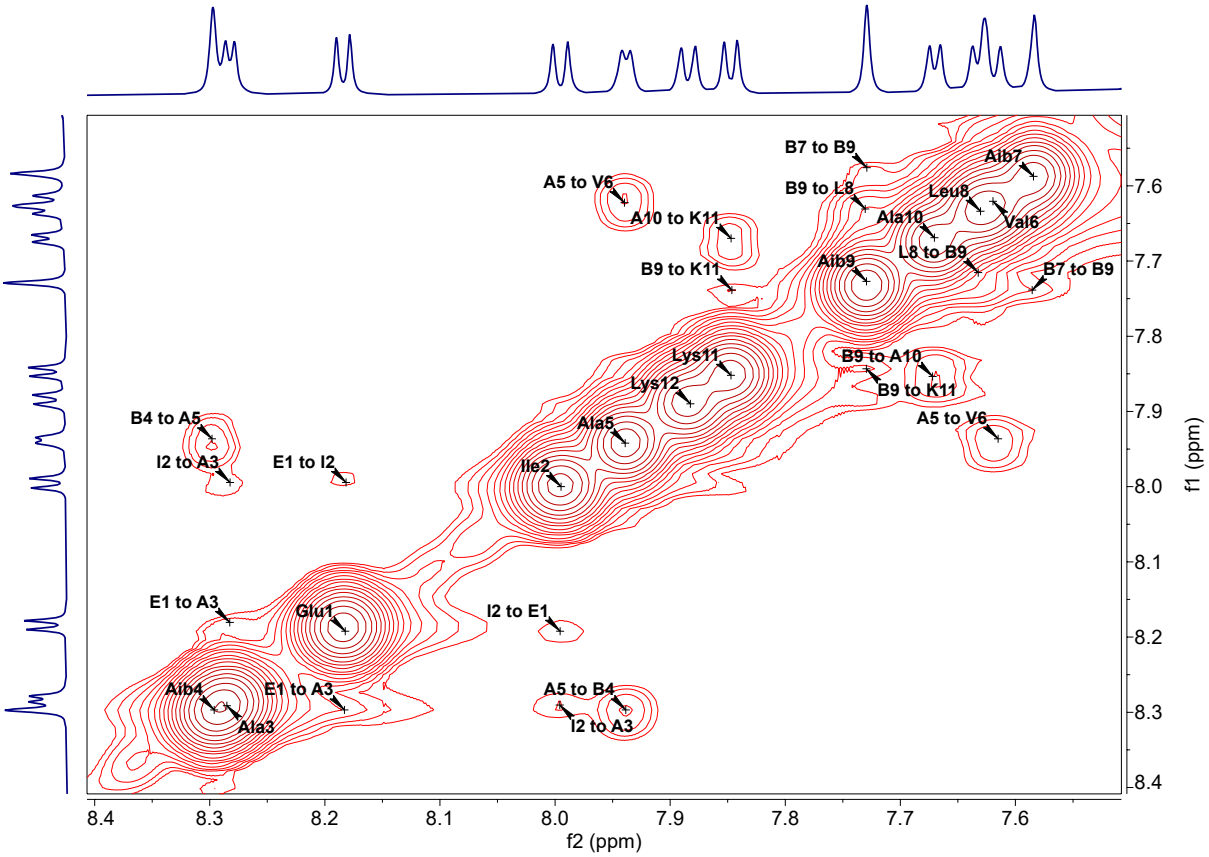

Figure S33. 2D NOESY spectrum of the K-alpha monomer in 90% H_2O, 10% D_2O (approximately 10 mM), with solvent suppression, obtained on a 600 MHz spectrometer at 25 ºC. The spectrum is zoomed into the amide NH region, with some visible NOE peaks that correspond to adjacent amide NHs (*i*, *i*+1) consistent with residual helicity (e.g. 10% as observed by circular dichroism spectroscopy). Labels indicate the amino acid residue of the corresponding amide NH peak.

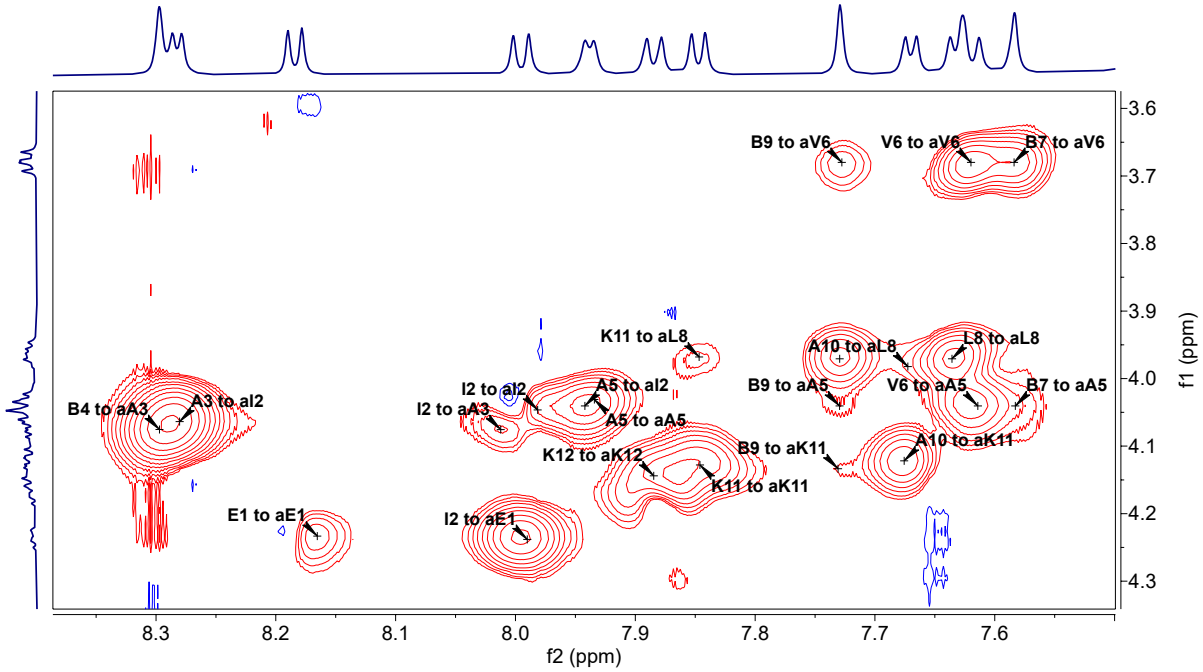

Figure S34. 2D NOESY spectrum of the K-alpha monomer in 90% H_2O, 10% D_2O (approximately 10 mM), with solvent suppression, obtained on a 600 MHz spectrometer at 25 ºC. This figure shows NOE correlations between NH amide peaks in f2 to αH peaks in f1, and are labelled accordingly. NOEs can be distinguished between (*i*, *i*+1), (*i*, *i* +2), and (*i*, *i* +3) residues, but with only one visible (*i*, *i* +4) NOE (B4 to αH of A5), consistent with the weak helicity observed by CD spectroscopy of the K-alpha monomer in aqueous solution.

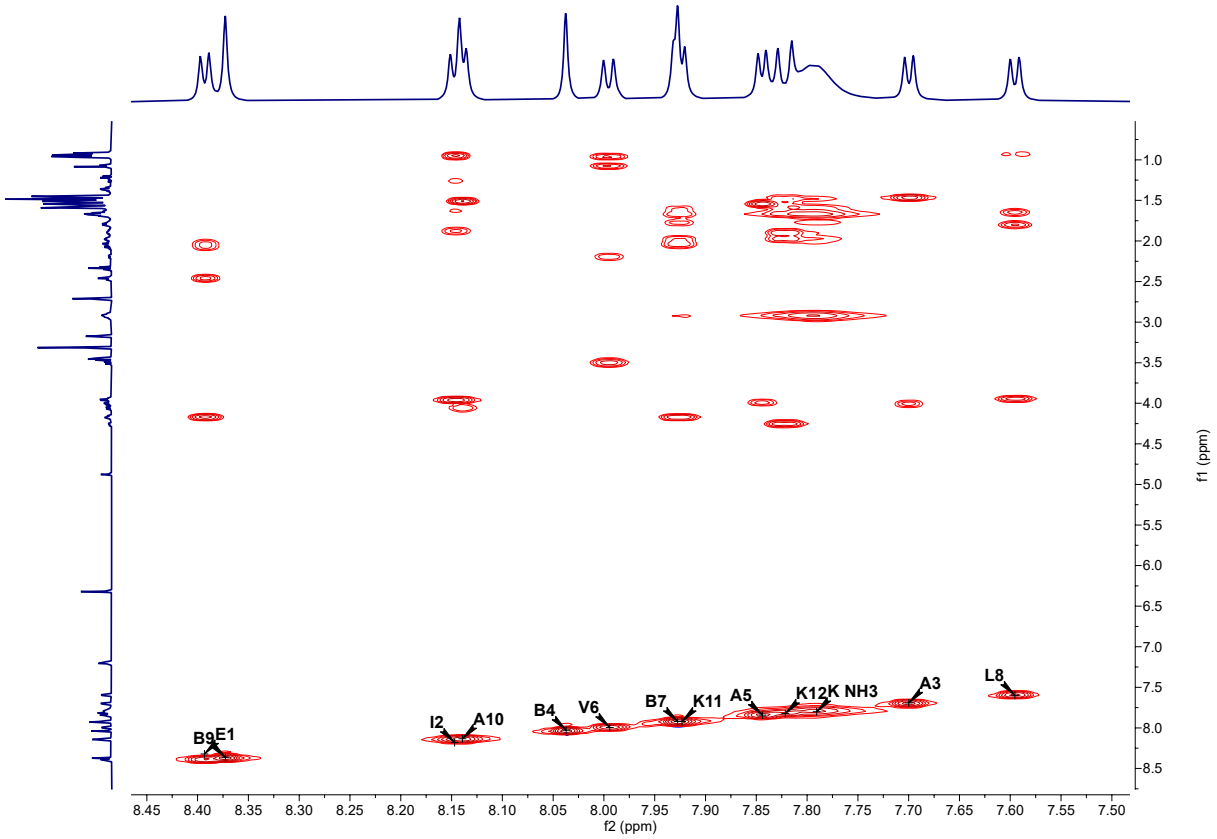

Figure S35. 2D TOCSY spectrum of the K-alpha monomer in 100% CD_3OH (approximately 10 mM), with solvent suppression, obtained on a 600 MHz spectrometer at 25 ºC. Labels indicate the amino acid residue of the corresponding amide NH peak. The figure highlights in particular the diagonal peaks in the NH amide region and cross-peaks of these NH peaks with the αH and side chain moieties.

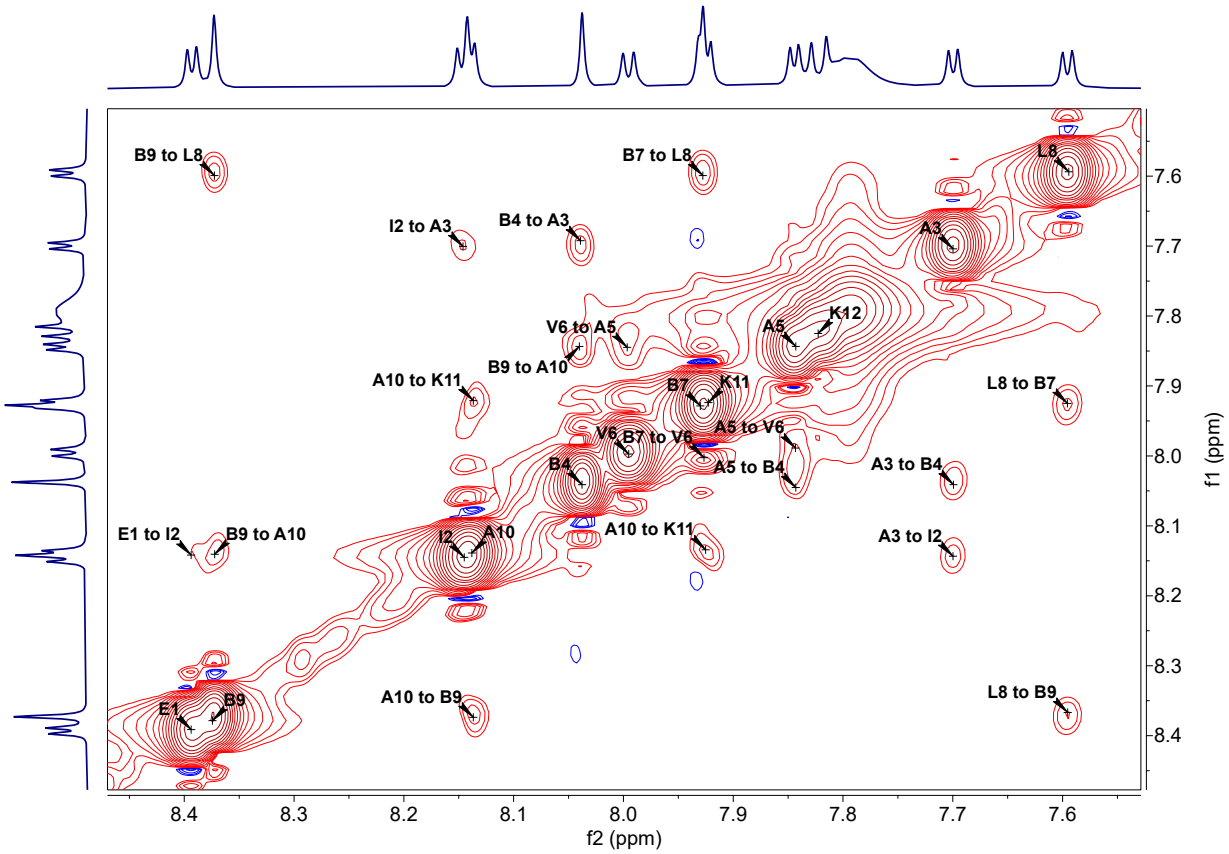

Figure S36. 2D NOESY spectrum of the K-alpha monomer in CD_3OH (approximately 10 mM with respect to peptide monomer concentration), with solvent suppression, obtained on a 600 MHz spectrometer at 25 ºC. The spectrum is zoomed into the amide NH region, revealing NOE peaks that correspond to adjacent amide NHs (*i*, *i*+1) consistent with a helical fold. Labels indicate the amino acid residue of the corresponding amide NH peak.

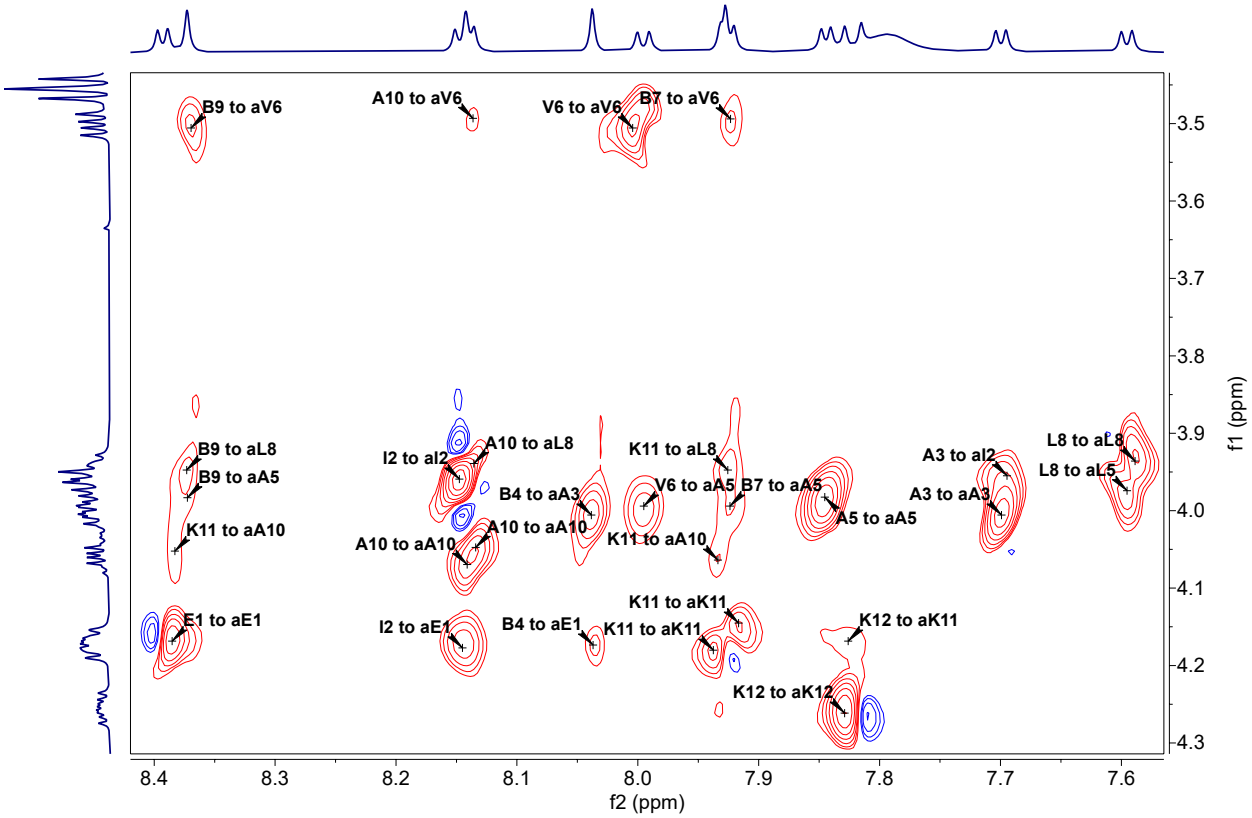

Figure S37. 2D NOESY spectrum of the K-alpha monomer in 100% CD_3OH (approximately 10 mM), with solvent suppression, obtained on a 600 MHz spectrometer at 25 ºC. This figure shows NOE correlations between NH amide peaks in f2 to αH peaks in f1, and are labelled accordingly. NOEs can be distinguished between (*i*, *i*+1), (*i*, *i* +2), (*i*, *i* +3), and (*i*, *i* +4) residues, with those to V6 (~3.5 ppm in f1) showing this trend in particular. This pattern of NOEs are consistent with helical folding.

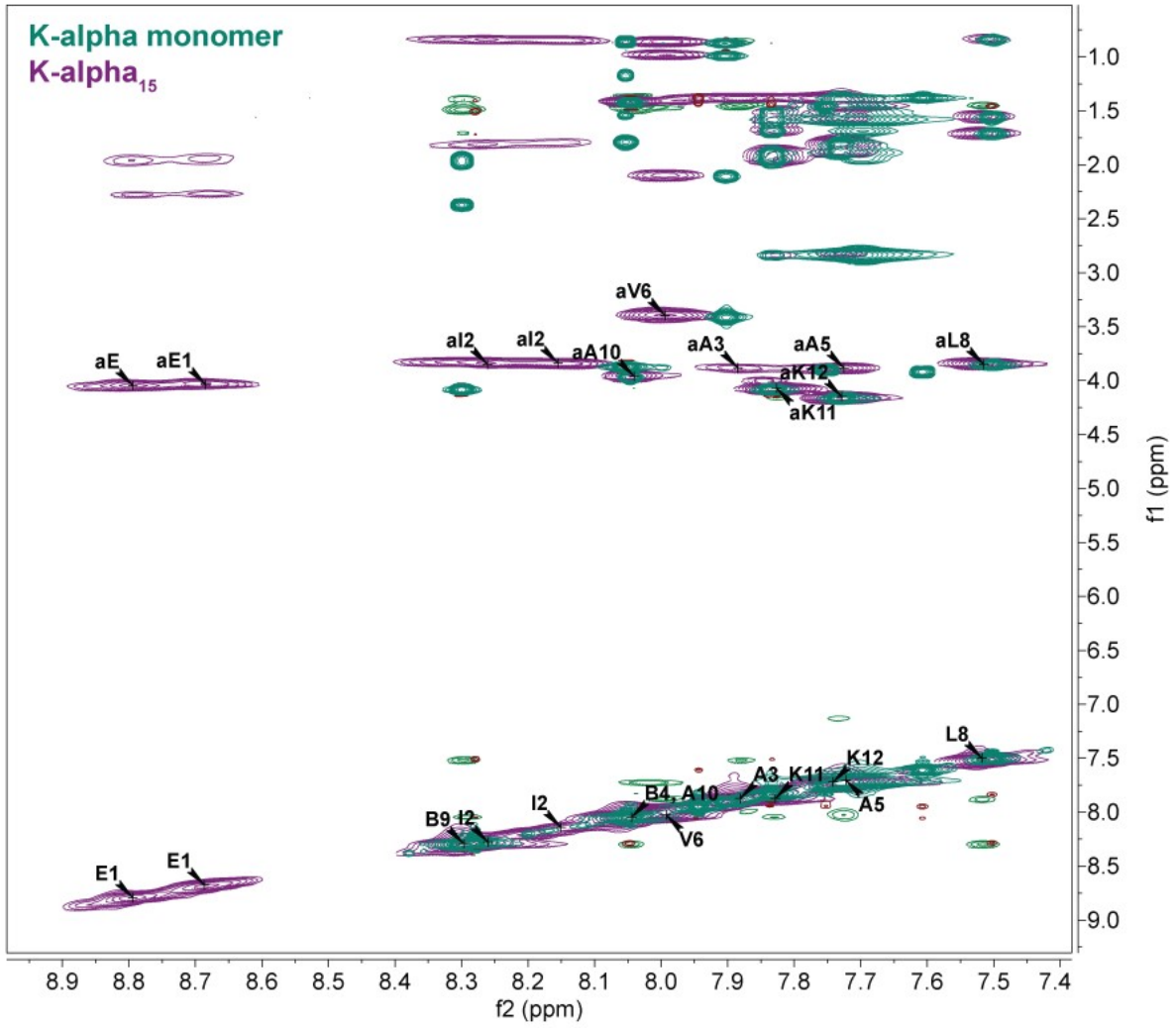

Figure S38. Overlaid 2D TOCSY spectra of the K-alpha monomer (green trace) and K-alpha$_{15}$ polymer (purple trace) in CD_3OH (approximately 10 and 5 mM peptide monomer concentration respectively), with solvent suppression, obtained on a 600 MHz spectrometer at 25 ºC. The figure highlights in particular the diagonal peaks in the NH amide region and cross-peaks of these NH peaks with the αH and side chain moieties. Black labels are indicated only for polymer peaks. The overlay supports that while some amino acids have similar chemical shifts in the peptide monomer and polymer samples (e.g. L8, K11, K12, and A10), others shift drastically (e.g. E1, I2, A3, V6).

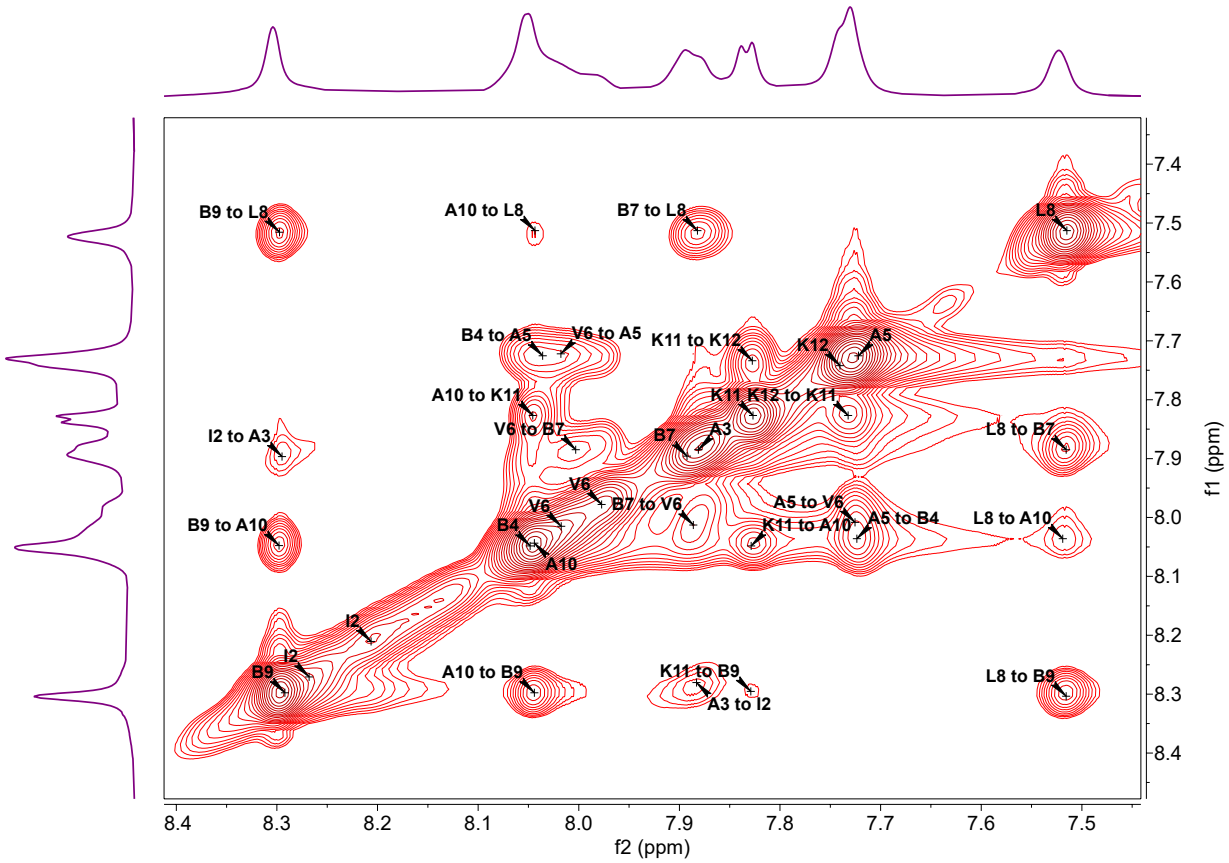

Figure S39. 2D NOESY spectrum of the K-alpha$_{15}$ polymer in CD_3OH (approximately 5 mM with respect to peptide monomer concentration), with solvent suppression, obtained on a 600 MHz spectrometer at 25 ºC. The spectrum is zoomed into the amide NH region, revealing NOE peaks that correspond to adjacent amide NHs (*i*, *i*+1) consistent with a helical fold, as well as several additional NOEs corresponding to more distant features (*i*, *i*+2) that further corroborate the helicity of the system. Labels indicate the amino acid residue of the corresponding amide NH peak.

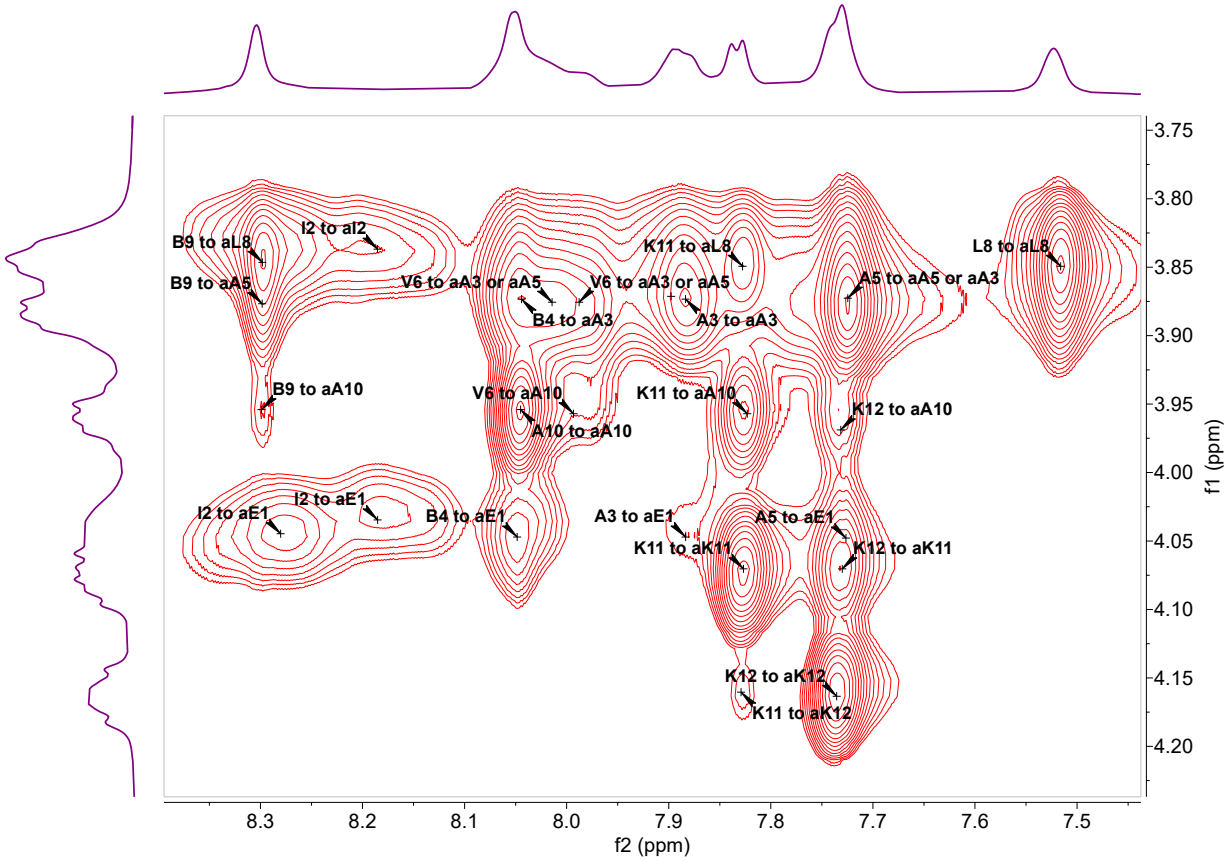

Figure S40. 2D NOESY spectrum of the K-alpha$_{15}$ polymer in CD_3OH (approximately 5 mM with respect to peptide monomer concentration), with solvent suppression, obtained on a 600 MHz spectrometer at 25 ºC. This inset shows NOE correlations between NH amide peaks in f2 to αH peaks in f1, and are labelled accordingly. NOEs can be distinguished between (*i*, *i*+1), (*i*, *i* +2), (*i*, *i* +3), and (*i*, *i* +4) residues.

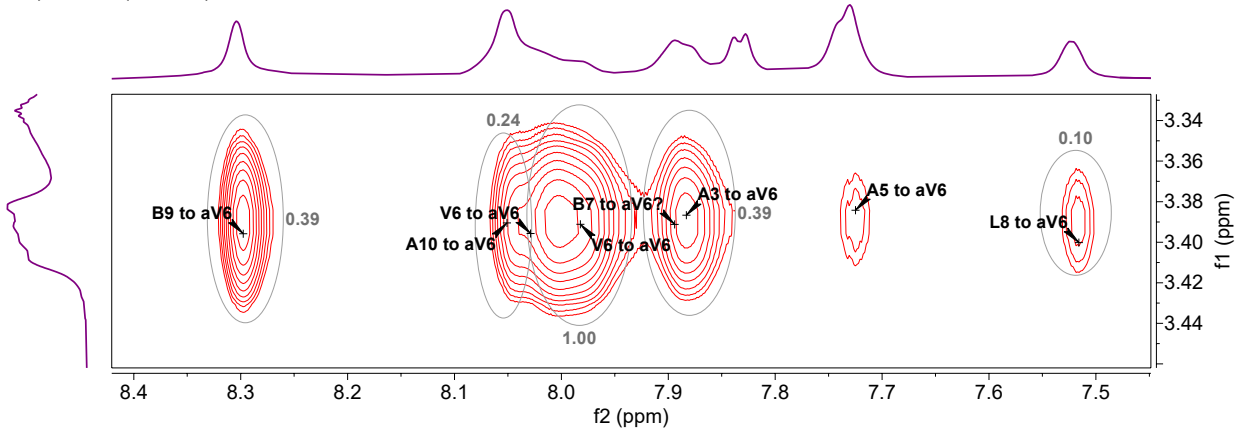

Figure S41. 2D NOESY spectrum of the K-alpha$_{15}$ polymer in CD_3OH (approximately 5 mM with respect to peptide monomer concentration), with solvent suppression, obtained on a 600 MHz spectrometer at 25 ºC. This inset shows NOE correlations between NH amide peaks in f2 to the αH peak of V6 in f1, and are labeled accordingly. NOEs can be distinguished between (*i*, *i*+1), (*i*, *i* +2), (*i*, *i* +3), and (*i*, *i* +4) residues, with integration indicating intensity approximately in the order of (I, i) > (*i*, *i* +1) ~ (*i*, *i* +3) > (*i*, *i* +4) ~ (*i*, *i* +2).

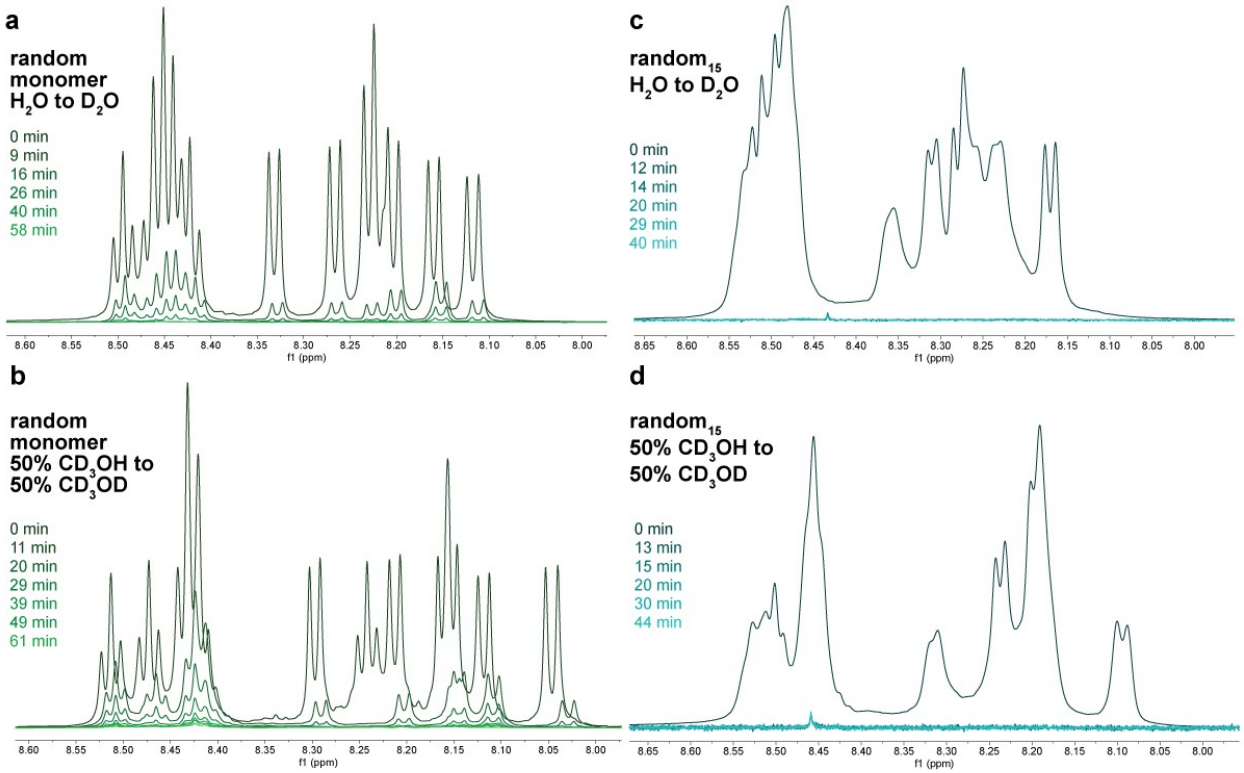

Figure S42. ^{1}H NMR spectroscopy data monitoring the disappearance of NH peaks of samples when dissolved in deuterated solvent (pure D_2O or 50% CD_3OD in D_2O), compared to spectra of the samples dissolved in 90% H_2O and 10% D_2O (a and c), or 50% CD_3OH with H_2O (b and d). The random monomer (a in water and b in 50% methanol) show slower exchange with solvent as compared to the random$_{15}$ polymer (c and d in water and 50% methanol respectively).

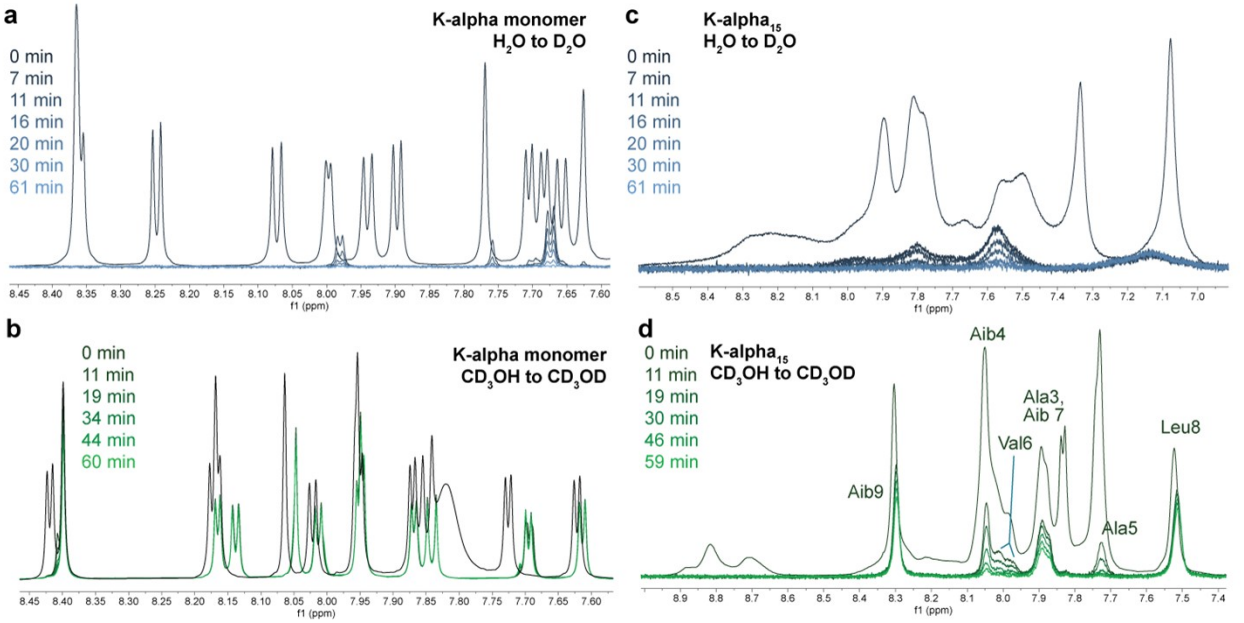

Figure S43. ^{1}H NMR spectroscopy data monitoring the disappearance of NH peaks of samples when dissolved in deuterated solvent (pure D_2O or CD_3OD), compared to spectra of the samples

dissolved in 90% H_2O and 10% D_2O (a and c), or pure CD_3OH (b and d). Both the K-alpha monomer and K-alpha$_{15}$ polymer show much slower exchange in water as compared to methanol.

7. Small-Angle X-ray Scattering

SAXS experiments were conducted at Beamline 16ID of the National Synchrotron Light Source II, Brookhaven National Laboratory.[24,25] Samples were dissolved in water (random-based polymers) or buffered solutions (100 mM sodium carbonate- or sodium acetate-based buffers for E-alpha- and K-alpha-based polymers respectively) in concentrations ranging from 1.25 to 5 mg/mL, dialyzed for two days against the buffer solution using 3.5 kDa MWCO dialysis cassettes, filtered through 0.22 μM hydrophilic PTFE membrane filters, shipped to the beamline in sealed PCR plates, and then loaded into sample holders for measurement in a flow-through cell at the beamline station.[26] The wavelength used for data collection ranges from 0.8172 Å to 0.8202 Å and is indicated in figure captions and in Tables S4–S6. Sample data was recorded on three Pilatus3 detectors to capture an approximate q range of 0.006 $Å^{-1}$ to 3.2 $Å^{-1}$. Data processing and background subtractions are performed using Python as previously detailed.[24]

Additional SAXS experiments were conducted at the 5-ID-D beamline of the Dupont-Northwestern-Dow Collaborative Access Team (DND-CAT) at the Advanced Photon Source, Argonne National Laboratory. Samples of 1 to 5% w/v of peptide-brush polymer in solvent were prepared and loaded into 1.5 mm quartz capillaries. The capillaries were then sealed with epoxy to prevent solvent evaporation prior to data acquisition. Capillaries were loaded into a multicapillary holder and scattering patterns were acquired at room temperature. Two-dimensional scattering patterns were obtained from 10 exposures using a Rayonix MX170-HS CCD area detector using a 0.5 s exposure time to X-rays with a wavelength of $\lambda = 1.2398$ Å and a sample-to-detector distance of 8.5 m. The 2D data were azimuthally averaged to yield 1D scattering patterns as intensity versus q. Incoherent background scattering was measured by acquiring scattering patterns for a solvent-loaded capillary in the absence of polymer samples.

Background-subtracted patterns were used to construct Kratky and Guinier plots. Specifically, Guinier plots were used to extract experimental radii of gyration, R_g, and the intensity at zero scattering angle, I_0, using the program ATSAS.[27] These values are reported in Tables S4, S5, and S6. Additionally, the values obtained from this analysis were used to generate Kratky and normalized Kratky plots of the corresponding data, which are presented in the manuscript and below (Figs. 5, S38, and S41). Fitting of the power law, Guinier-Porod,[28,29] and flexible cylinder models[30,31] was performed using SasView.[32] These models are frequently used for similar bottle-brush polymers and provide detail into their conformations in solution.[33–38] For example, shorter polymers often collapse into compact, globular conformations, which typically have a dimension (or shape) parameter s of 0 and a Porod exponent of 4, whereas more anisotropic systems will yield dimension parameters closer to 1. We observe that as polymer lengths increase, the values of s determined also increase.

Additionally, as bottlebrush polymers extend in length to become more rod-like and less liable to collapse into small globular structures, their scattering patterns often display multiple power law dependences, i.e. Q^0, Q^{-1}, and Q^{-4}, which correspond to the radius of the rod, the length of the rod, and the surface of the rod. We note this tendency in particular for the scattering data of the random$_{90}$ and E-alpha$_{90}$ polymers, which display excellent fits to three power law models with

coefficients that closely match these values. The normalized Kratky plots of these two polymers also significantly deviate from values expected for a compact sphere. We note literature on the interpretation of Kratky plots of disordered proteins, which inspired us in the course of this study.[39,40] However, unlike in proteins where the relationship of protein chain length to R_g is well validated, in these brush polymer systems, additional validation outside of the scope of this work would be needed to utilize similar analyses.

Data for samples of all concentrations were generally examined for signs of aggregation or interparticle repulsion, and generally, the data of the intermediate concentration, 2.5 mg/mL, was chosen due to not exhibiting such effects while maintaining high intensities and signal-to-noise.

Table S4. Table of structural parameters of α-helical peptide-based polymers derived from the E-alpha peptide monomer. All R_g and I_0 values were derived from samples of concentrations 2.5 mg polymer per mL of solvent.

Sample Name	Solvent	λ (Å)	R_g (nm), from Guinier plot fit	I_0	Fidelity
E-alpha$_7$	Aqueous buffer[a]	0.8172	2.24 ± 0.01	5.90 ± 0.03	1
E-alpha$_{15}$	Aqueous buffer[a]	0.8172	2.24 ± 0.01	7.81 ± 0.03	1
E-alpha$_{30}$	Aqueous buffer[a]	0.8172	2.82 ± 0.02	12.12 ± 0.05	0.94
E-alpha$_{45}$	Aqueous buffer[a]	0.8172	3.24 ± 0.02	15.77 ± 0.05	0.98
E-alpha$_{90}$	Aqueous buffer[a]	0.8172	6.92 ± 0.04	66.7 ± 0.3	0.88
E-alpha$_7$	50% MeOH[b]	0.8202	2.12 ± 0.04	0.800 ± 0.009	0.98
E-alpha$_{15}$	50% MeOH[b]	0.8202	2.82 ± 0.04	2.29 ± 0.03	0.30
E-alpha$_{30}$	50% MeOH[b]	0.8202	3.33 ± 0.03	4.79 ± 0.02	0.96
E-alpha$_{45}$	50% MeOH[b]	0.8202	4.56 ± 0.07	5.75 ± 0.06	0.23
E-alpha$_{90}$	50% MeOH[b]	0.8202	9.2 ± 0.1	41.0 ± 0.4	0.46
E-alpha$_{15}$	100% MeOH[c]	1.2398	2.46 ± 0.02	0.14 ± 0.01	1.00
E-alpha$_{30}$	100% MeOH[c]	1.2398	3.47 ± 0.08	0.33 ± 0.01	1.00
E-alpha$_{45}$	100% MeOH[c]	1.2398	4.49 ± 0.01	0.67 ± 0.01	1.00

[a] 100 mM Na_2CO_3 buffer, pH 10.
[b] 50% MeOH (v/v) with 50 mM Na_2CO_3 buffer.
[c] 100% MeOH with 3 mM NaOH (to enable sample solubility).

Table S5. Table of structural parameters of α-helical peptide-based polymers derived from the K-alpha peptide monomer. Unless otherwise stated, all R_g and I_0 values were derived from samples of concentrations of 2.5 mg polymer per mL of solvent.

Sample Name	Solvent	λ (Å)	R_g (nm), from Guinier plot fit	I_0	Fidelity
K-alpha$_{15}$	Aqueous buffer[a]	0.8202	2.07 ± 0.04	0.470 ± 0.005	0.99
K-alpha$_{30}$	Aqueous buffer[a,b]	0.8203	2.35 ± 0.03	1.47 ± 0.02	1
K-alpha$_{45}$	Aqueous buffer[a]	0.8202	2.89 ± 0.05	1.03 ± 0.01	0.92
K-alpha$_{15}$	50% MeOH[c]	0.8202	2.15 ± 0.02	1.220 ± 0.006	1.00
K-alpha$_{30}$	50% MeOH[c,d]	0.8202	2.58 ± 0.04	6.16 ± 0.07	0.83
K-alpha$_{45}$	50% MeOH[c]	0.8202	3.40 ± 0.03	4.02 ± 0.03	0.63

[a] 100 mM NaOAc buffer, pH 4.
[b] 1.25 mg/mL
[c] 50% MeOH (v/v) with 50 mM NaOAc buffer.
[d] 5.0 mg/mL

Table S6. Table of structural parameters of random coil peptide-based polymers. All R_g and I_0 values were derived from samples that consisted of 2.5 mg polymer per mL of solvent.

Sample Name	Solvent	λ (Å)	R_g (nm), from Guinier plot fit	I_0	Fidelity
random$_{15}$	Water	0.8172	2.42 ± 0.02	12.24 ± 0.05	0.81
random$_{30}$	Water	0.8172	2.483 ± 0.008	16.31 ± 0.04	1.0
random$_{45}$	Water	0.8172	3.32 ± 0.01	30.46 ± 0.06	0.92
random$_{90}$	Water	0.8180	5.40 ± 0.06	4.06 ± 0.03	0.98
random$_{15}$	50% MeOH	0.8202	2.56 ± 0.02	4.57 ± 0.03	0.98
random$_{30}$	50% MeOH	0.8202	3.03 ± 0.01	10.33 ± 0.03	0.67
random$_{45}$	50% MeOH	0.8202	3.47 ± 0.04	11.46 ± 0.08	0.56

Table S7. Table of structural parameters of α-helical peptide-based polymers derived from the E-alpha peptide sequence. Specifically, we report the radius of gyration R_g, the dimension variable *s*, and the Porod exponent *d* determined from Guinier-Porod model[28,29] fits performed in SasView,[32] along with the goodness-of-fit values.

Sample Name	Solvent	R_g (nm)	*s*	*d* (Porod exponent)	χ^2
E-alpha$_7$	Aqueous buffer[a]	2.16 ± 0.02	0.05 ± 0.01	4.48 ± 0.4	0.84
E-alpha$_{15}$	Aqueous buffer[a]	2.232 ± 0.008	~0 (4×10^{-19})	4.1 ± 0.2	0.87
E-alpha$_{30}$	Aqueous buffer[a]	2.71 ± 0.02	0.033 ± 0.008	3.6 ± 0.1	0.93
E-alpha$_{45}$	Aqueous buffer[a]	2.97 ± 0.01	0.085 ± 0.007	3.24 ± 0.06	1.63
E-alpha$_{90}$	Aqueous buffer[a]	3.63 ± 0.03	0.569 ± 0.008	2.074 ± 0.008	27
E-alpha$_7$	50% MeOH[b]	1.70 ± 0.03	0.28 ± 0.02	3.7 ± 0.4	1.04
E-alpha$_{15}$	50% MeOH[b]	2.15 ± 0.02	0.25 ± 0.01	4.4 ± 0.3	1.20
E-alpha$_{30}$	50% MeOH[b]	2.75 ± 0.03	0.23 ± 0.02	3.01 ± 0.05	2.28
E-alpha$_{45}$	50% MeOH[b]	2.50 ± 0.03	0.50 ± 0.02	3.08 ± 0.06	2.22
E-alpha$_{90}$	50% MeOH[b]	1.584 ± 0.008	1.202 ± 0.003	4.04 ± 0.11	1.61

Table S8. Table of structural parameters of α-helical peptide-based polymers derived from the E-alpha peptide monomer. P1, P2, and P3 designate power law coefficients derived from fitting the power law model as implemented in SasView, with the respective q range of the fit and goodness-of-fit value designated below the coefficient.[32]

Sample Name	Solvent	P1	P2	P3
$E\text{-alpha}_7$	Aqueous buffer[a]	0.1 ± 0.3 0.01 to 0.04 Å^{-1}; χ^2 0.60	3.8 ± 0.2 0.1 to 0.2 Å^{-1}; χ^2 1.79	
$E\text{-alpha}_{15}$	Aqueous buffer[a]	0.0017 ± 0.8 0.01 to 0.03 Å^{-1}; χ^2 0.59	3.5 ± 0.2 0.1 to 0.18 Å^{-1}; χ^2 0.72	
$E\text{-alpha}_{30}$	Aqueous buffer[a]	0.0014 ± 0.4 0.007 to 0.03 Å^{-1}; χ^2 0.74	3.99 ± 0.06 0.08 to 0.25 Å^{-1}; χ^2 1.79	
$E\text{-alpha}_{45}$	Aqueous buffer[a]	0.0009 ± 0.2 0.008 to 0.03 Å^{-1}; χ^2 1.44	4.02 ± 0.06 0.08 to 0.25 Å^{-1}; χ^2 1.04	
$E\text{-alpha}_{90}$	Aqueous buffer[a]	0.0019 ± 0.4 0.007 to 0.015 Å^{-1}; χ^2 0.70	1.08 ± 0.02 0.02 to 0.05 Å^{-1}; χ^2 4.73	3.86 ± 0.06 0.08 to 0.25 Å^{-1}; χ^2 0.86
$E\text{-alpha}_7$	50% MeOH[b]	0.1 ± 0.2 0.02 to 0.06 Å^{-1}; χ^2 0.43	2.1 ± 0.1 0.08 to 0.2 Å^{-1}; χ^2 1.06	
$E\text{-alpha}_{15}$	50% MeOH[b]	0.05 ± 0.08 0.012 to 0.05 Å^{-1}; χ^2 1.04	2.7 ± 0.1 0.08 to 0.15 Å^{-1}; χ^2 1.40	
$E\text{-alpha}_{30}$	50% MeOH[b]	0 ± 3 0.007 to 0.02 Å^{-1}; χ^2 0.72	2.30 ± 0.06 0.06 to 0.12 Å^{-1}; χ^2 1.59	
$E\text{-alpha}_{45}$	50% MeOH[b]	0.0 ± 0.6 0.009 to 0.02 Å^{-1}; χ^2 0.96	3.24 ± 0.06 0.07 to 0.18 Å^{-1}; χ^2 1.44	
$E\text{-alpha}_{90}$	50% MeOH[b]	0.1 ± 0.1 0.005 to 0.015 Å^{-1}; χ^2 1.05	1.08 ± 0.02 0.02 to 0.05 Å^{-1}; χ^2 2.19	3.62 ± 0.03 0.08 to 0.2 Å^{-1}; χ^2 4.57

[a] 100 mM Na_2CO_3 buffer.

[b] 50% MeOH (v/v) with 50 mM Na_2CO_3 buffer.

Table S9. Table of structural parameters of α-helical peptide-based polymers derived from the E-alpha peptide monomer. Specifically, we report the parameters determined using the flexible cylinder model[30,31] as implemented in SasView,[32] with *L* representing the length of the flexible cylinder, the Kuhn length of the flexible cylinder, *R* as the radius of the flexible cylinder, as well as the polydispersity of *R* and the goodness-of-fit parameter χ^2.

Sample Name	Solvent	*L* (nm)	Kuhn Length (nm)	*R* (nm)	Polydispersity of *R*	χ^2
E-alpha$_7$	Aqueous buffer[a]	6.7 ± 0.4	3.8 ± 0.2	1.82 ± 0.02	0.21 ± 0.03	0.79
E-alpha$_{15}$	Aqueous buffer[a]	7.2 ± 0.3	3.7 ± 0.1	1.80 ± 0.01	0.21 ± 0.02	0.58
E-alpha$_{30}$	Aqueous buffer[a]	8.7 ± 0.3	4.8 ± 0.1	2.15 ± 0.02	0.28 ± 0.02	0.73
E-alpha$_{45}$	Aqueous buffer[a]	11.9 ± 0.3	5.3 ± 0.2	2.16 ± 0.02	0.33 ± 0.02	0.71
E-alpha$_{90}$	Aqueous buffer[a]	32.3 ± 0.4	13.4 ± 0.2	2.27 ± 0.02	0.40 ± 0.01	1.98
E-alpha$_7$	50% MeOH[b]	14.0 ± 0.3	1.4 ± 0.4	1.5 ± 0.6	–	0.73
E-alpha$_{15}$	50% MeOH[b]	16.79 ± 0.02	1.7 ± 0.2	1.80 ± 0.04	0.16 ± 0.03	3.77
E-alpha$_{30}$	50% MeOH[b]	17 ± 2	3.3 ± 0.9	1.94 ± 0.06	0.35 ± 0.03	0.68
E-alpha$_{45}$	50% MeOH[b]	28.27 ± 0.02	2.8 ± 0.2	1.7 ± 0.2	0.4 ± 0.1	2.71
E-alpha$_{90}$	50% MeOH[b]	38.4 ± 0.2	20.4 ± 0.1	2.04 ± 0.02	0.40 ± 0.01	2.96

[a] 100 mM Na_2CO_3 buffer.
[b] 50% MeOH (v/v) with 50 mM Na_2CO_3 buffer.

Table S10. Table of structural parameters of random coil peptide-based polymers. Specifically, we report the radius of gyration R_g, the dimension variable *s*, and the Porod exponent *d* determined from Guinier-Porod model[28,29] fits performed in SasView,[32] along with the goodness-of-fit values.

Sample Name	Solvent	R_g (nm)	*s*	*d* (Porod exponent)	χ^2
random$_{15}$	H_2O	2.136 ± 0.007	0.102 ± 0.005	5.9 ± 0.2	0.46
random$_{30}$	H_2O	2.43 ± 0.02	0.014 ± 0.007	4.7 ± 0.3	0.48
random$_{45}$	H_2O	2.703 ± 0.009	0.135 ± 0.004	2.350 ± 0.003	7.36
random$_{90}$	H_2O	1.83 ± 0.03	1.00 ± 0.01	6 ± 2	6.27
random$_{15}$	50% MeOH	1.92 ± 0.04	0.16 ± 0.01	2.6 ± 0.3	0.58
random$_{30}$	50% MeOH	2.188 ± 0.009	0.310 ± 0.004	3.37 ± 0.08	5.03
random$_{45}$	50% MeOH	2.68 ± 0.01	0.224 ± 0.008	3.92 ± 0.07	2.67

Table S11. Table of structural parameters of random coil peptide-based polymers. Specifically, we report the parameters determined using the flexible cylinder model[30,31] as implemented in SasView,[32] with *L* representing the length and *R* as the radius of the cylinder, as well parameters for the polydispersity of *R*, the Kuhn length of the cylinder, and the goodness-of-fit parameter χ^2.

Sample Name	Solvent	*L* (nm)	Kuhn Length (nm)	*R* (nm)	Polydispersity of *R*	χ^2
$random_{15}$	H_2O	6 ± 3	2.9 ± 0.2	1.8 ± 0.2	0.35 ± 0.07	1.49
$random_{30}$	H_2O	5.0 ± 0.5	3.1 ± 0.2	2.35 ± 0.03	0.18 ± 0.02	0.50
$random_{45}$	H_2O	15.454 ± 0.0002	3.9 ± 0.1	2.136 ± 0.008	0.19 ± 0.01	0.91
$random_{90}$	H_2O	20.5 ± 0.5	15.1 ± 0.6	2.26 ± 0.03	0.22 ± 0.03	0.66
$random_{15}$	50% MeOH	9.7 ± 0.4	3.4 ± 0.5	1.73 ± 0.09	–	0.89
$random_{30}$	50% MeOH	14.1550 ± 0.0002	3.5 ± 0.1	1.956 ± 0.005	0.135 ± 0.009	11.1
$random_{45}$	50% MeOH	21.80 ± 0.02	2.2 ± 0.2	2.09 ± 0.06	0.19 ± 0.03	1.32

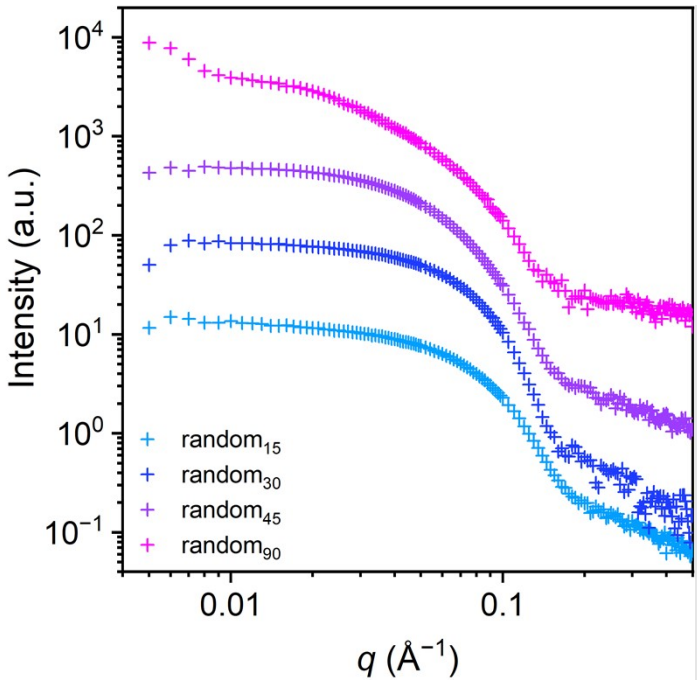

Figure S44. Background-subtracted small-angle X-ray scattering patterns of solutions of different lengths of random coil-based polymers, with concentrations of 2.5 mg/mL in water. The polymers $random_{15}$, $random_{30}$, $random_{45}$, and $random_{90}$ are indicated with azure, dark blue, purple, and magenta tick marks respectively. The wavelength of measurement was 0.8172 Å; $random_{90}$ was measured at a wavelength of 0.8180 Å. SAXS patterns are vertically offset from each other for greater visual clarity.

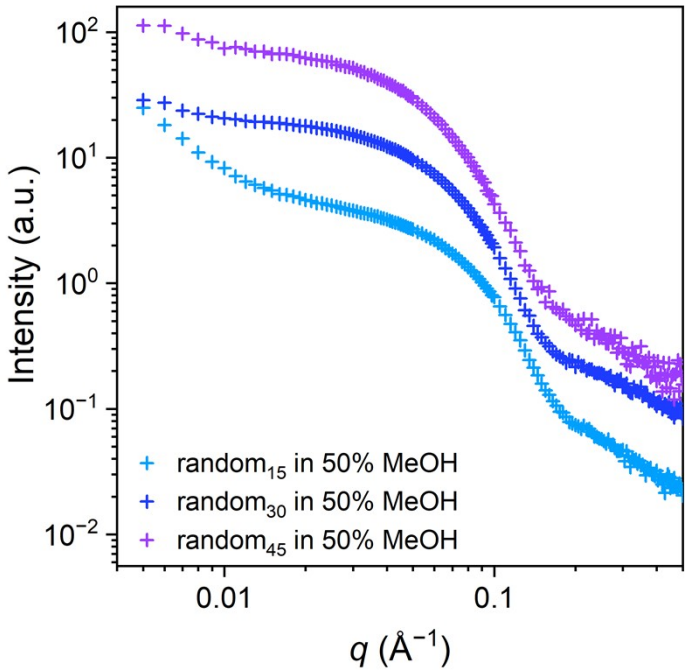

Figure S45. Background-subtracted small-angle X-ray scattering patterns of solutions of different lengths of random coil-based polymers (2.5 mg/mL) in 50% methanol (v/v). The polymers random$_{15}$, random$_{30}$, and random$_{45}$ are indicated with azure, dark blue, and purple tick marks respectively. The wavelength of measurement was 0.8202 Å. SAXS patterns are vertically offset from each other for greater visual clarity.

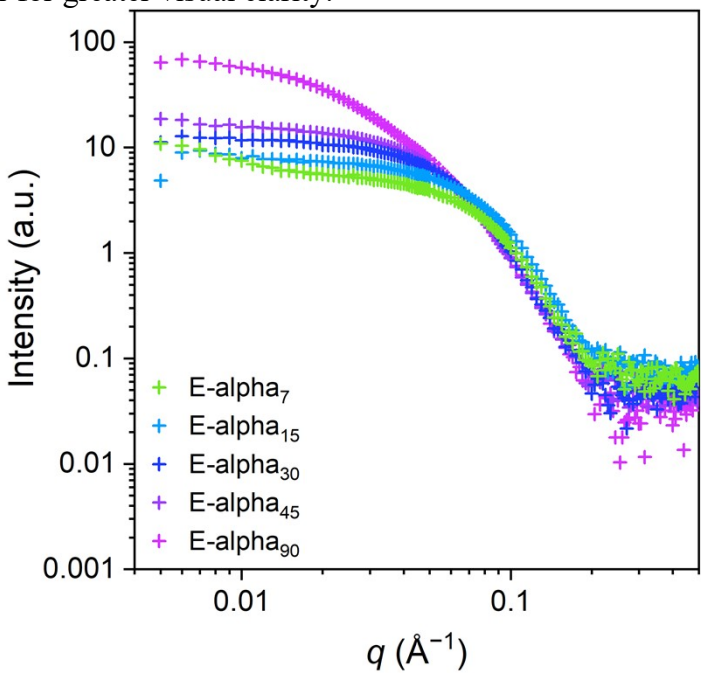

Figure S46. Background-subtracted small-angle X-ray scattering patterns of E-alpha helix-based polymers (2.5 mg/mL) in sodium carbonate buffer. The polymer E-alpha$_7$, E-alpha$_{15}$, E-alpha$_{30}$, E-alpha$_{45}$, and E-alpha$_{90}$ are indicated with green, azure, dark blue, purple, and magenta tick marks respectively. The wavelength of measurement was 0.8172 Å.

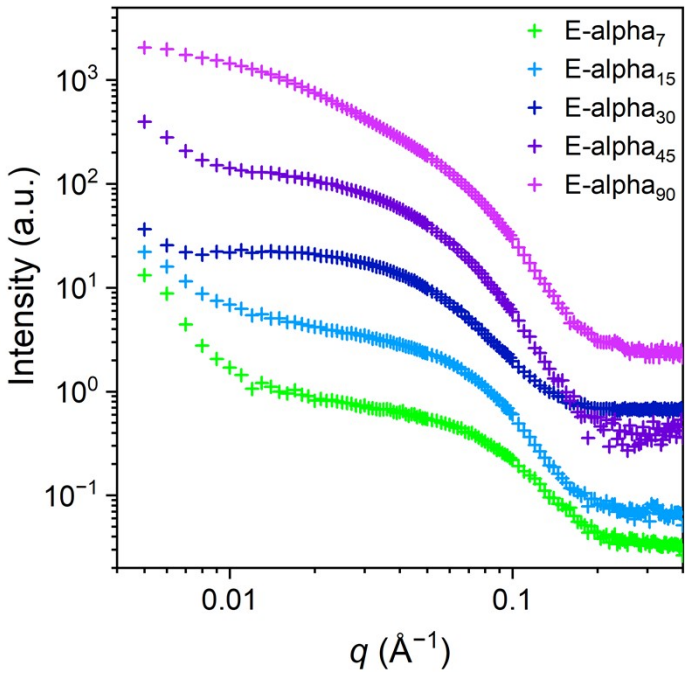

Figure S47. Background-subtracted SAXS patterns of solutions of E-alpha helix-based polymers (50% methanol and 50 mM sodium carbonate buffer). The polymers E-alpha$_7$, E-alpha$_{15}$, E-alpha$_{30}$, E-alpha$_{45}$, and E-alpha$_{90}$ are indicated with green, azure, dark blue, purple, and magenta tick marks respectively. The wavelength of measurement was 0.8202 Å. SAXS patterns are vertically offset from each other for greater visual clarity.

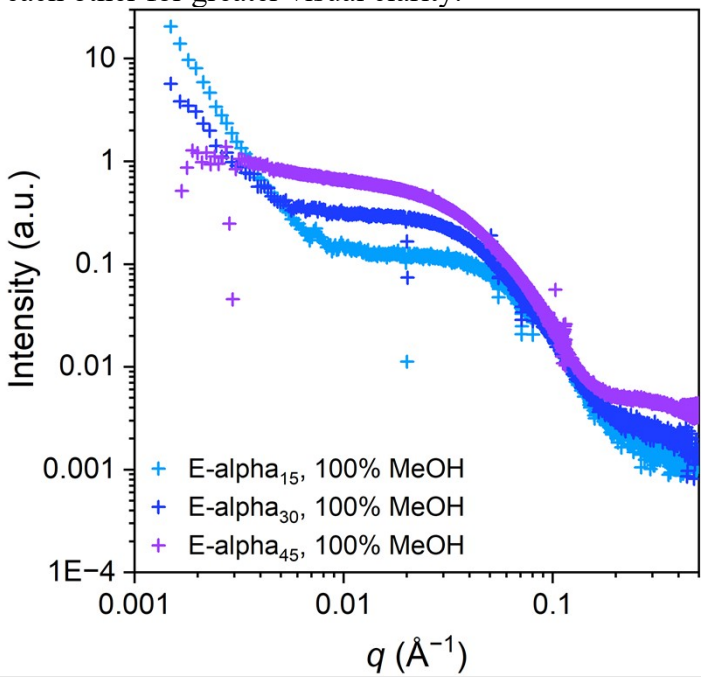

Figure S48. Background-subtracted SAXS data of solutions of E-alpha-based polymers (100% methanol with 3 mM NaOH). The polymers E-alpha$_{15}$, E-alpha$_{30}$, and E-alpha$_{45}$ are indicated with azure, dark blue, and purple tick marks respectively. The measurement wavelength was 1.2398 Å.

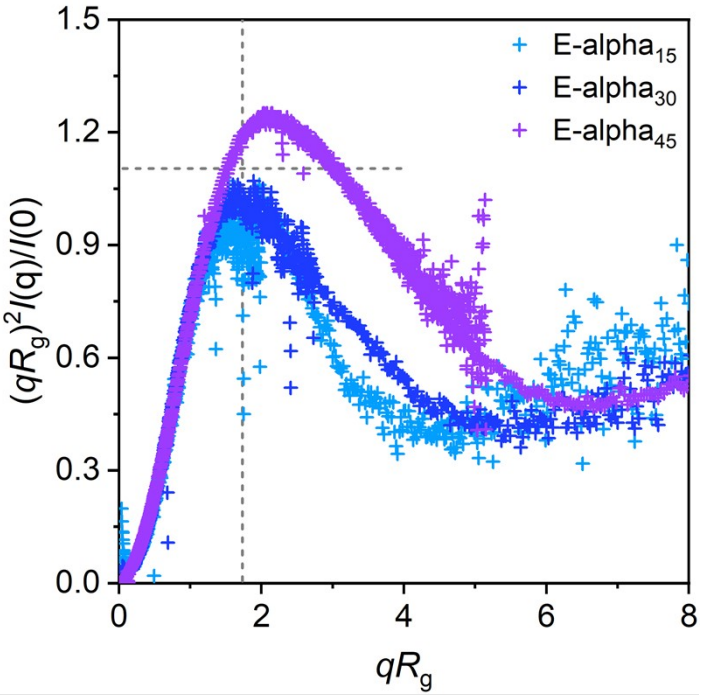

Figure S49. Normalized Kratky plots of background-subtracted SAXS data of solutions of E-alpha-based polymers (2.5 mg/mL in 100% methanol with 3 mM NaOH). The polymers E-alpha$_{15}$, E-alpha$_{30}$, and E-alpha$_{45}$ are indicated with azure, dark blue, and purple tick marks respectively. The wavelength of measurement was 1.2398 Å. Gray dashed lines indicate positions of qR_g and $(qR_g)2I_{(q)}/I_{(0)}$ for an ideal compact sphere.

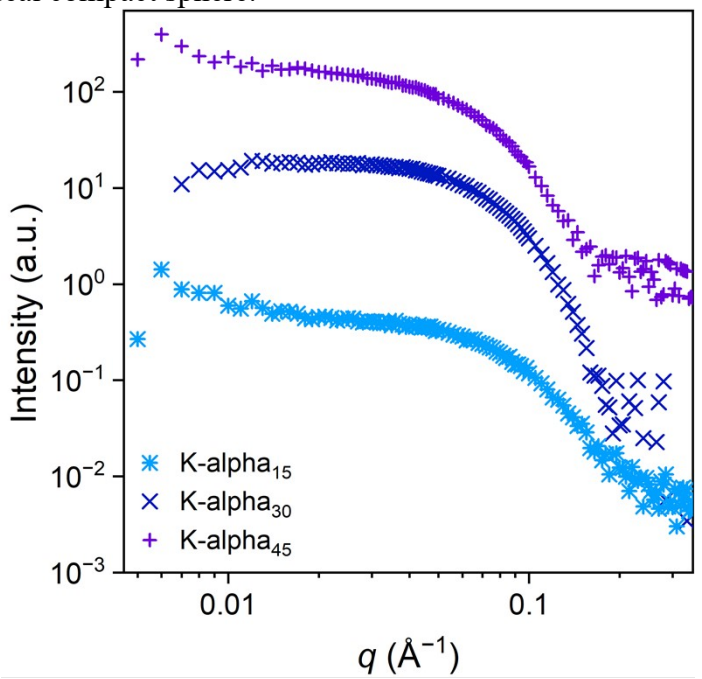

Figure S50. Background-subtracted SAXS patterns of solutions of K-alpha helix-based polymers (2.5 mg/mL in 100 mM sodium acetate buffer). The polymers K-alpha$_{15}$, K-alpha$_{30}$, and K-alpha$_{45}$ are indicated with azure, dark blue, and purple tick marks respectively. The wavelength

of measurement was 0.8202 Å; K-alpha$_{30}$ was measured at 0.8203 Å. SAXS patterns are vertically offset from each other for visual clarity.

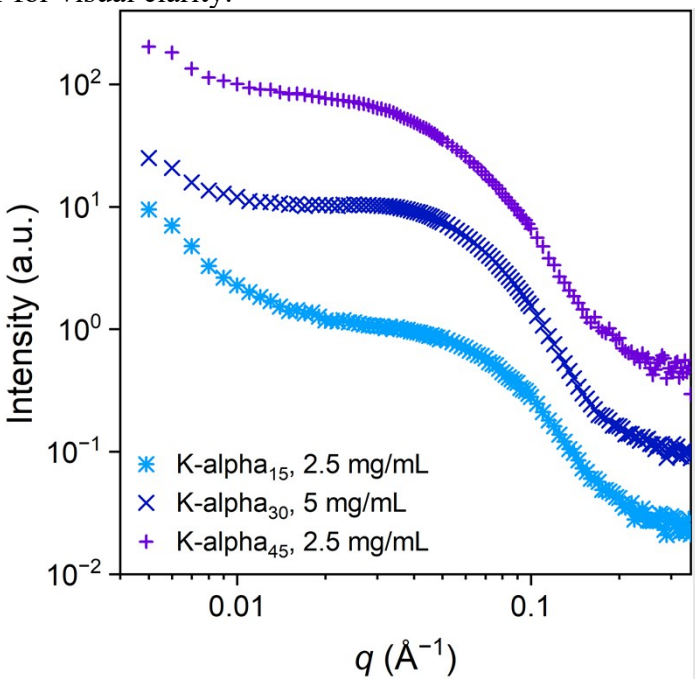

Figure S51. Background-subtracted small-angle X-ray scattering patterns of solutions of K-alpha-based polymers (50% methanol and 50 mM sodium acetate buffer). The polymers K-alpha$_{15}$, K-alpha$_{30}$, and K-alpha$_{45}$ are indicated with azure, dark blue, and purple tick marks respectively. The wavelength of measurement was 0.8202 Å. SAXS patterns are vertically offset from each other for greater visual clarity.

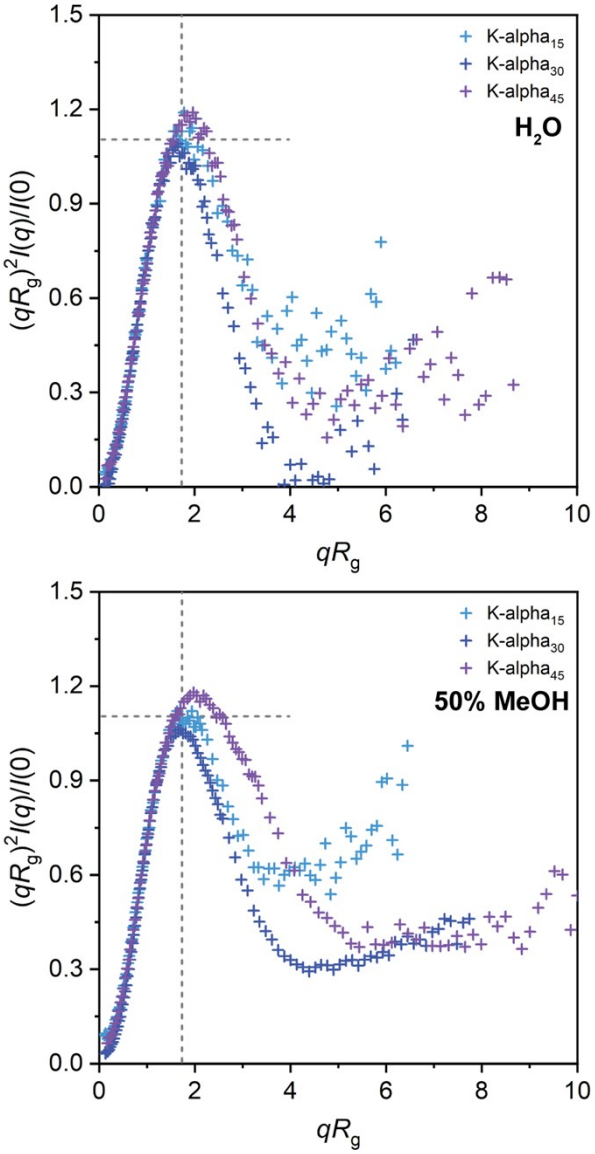

Figure S52. Normalized Kratky plots of background-subtracted SAXS data of solutions of K-alpha-based polymers (top: 100 mM sodium acetate buffer, bottom: 50% methanol (v/v) with 50 mM sodium acetate buffer). The polymers K-alpha$_{15}$, K-alpha$_{30}$, and K-alpha$_{45}$ are indicated with azure, dark blue, and purple tick marks respectively. The wavelength of measurement was generally 0.8202 Å, with E-alpha$_{30}$ in 100 mM sodium acetate measured with a wavelength of 0.8203 Å. Gray dashed lines indicate positions of qR_g and $(qR_g)2I_{(q)}/I_{(0)}$ for an ideal compact sphere.

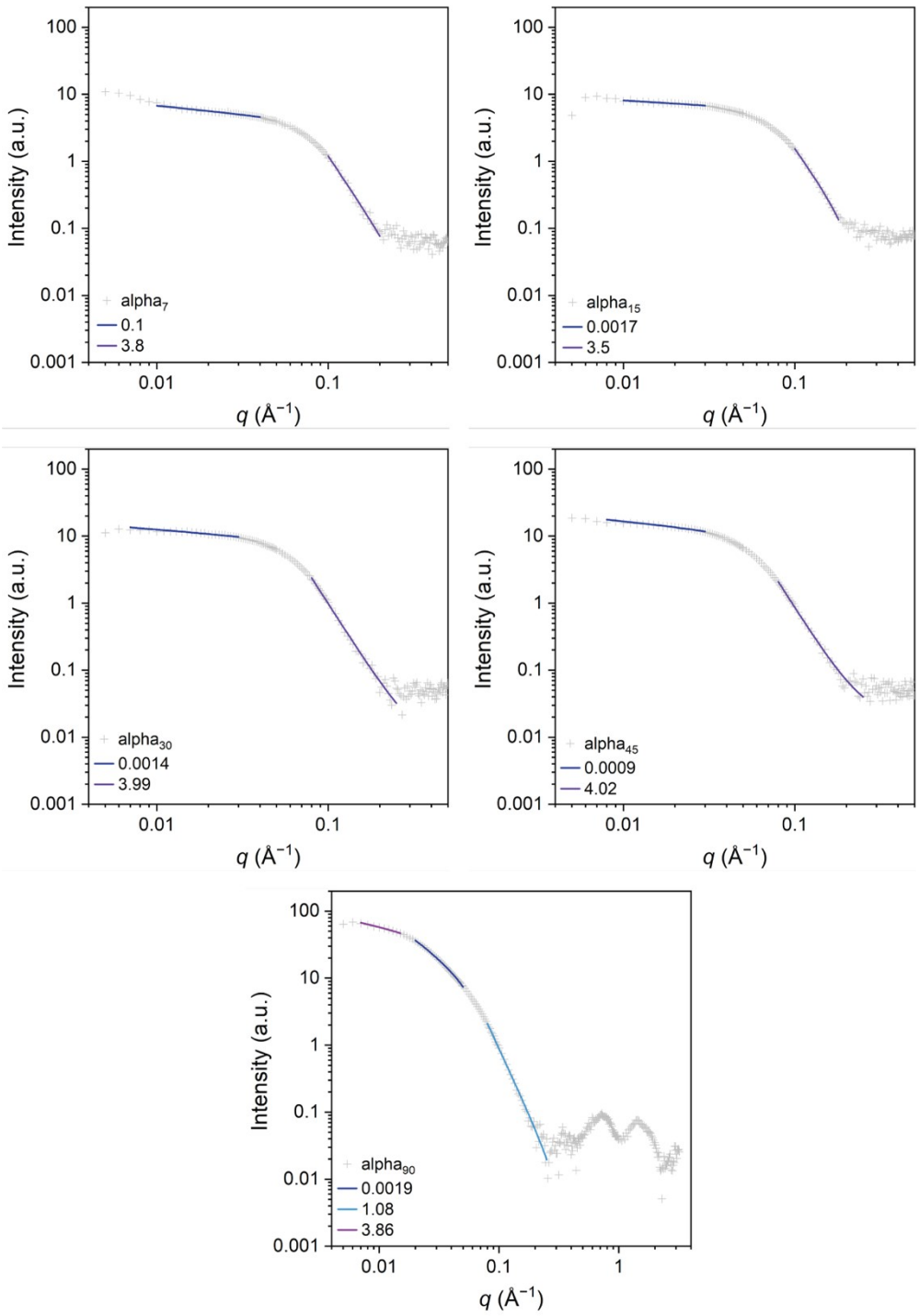

Figure S53. Background-subtracted small-angle X-ray scattering patterns of solutions of different lengths of E-alpha polymers (tick marks), with concentrations of 2.5 mg/mL in sodium carbonate buffer, compared to the power law fits (lines) as implemented in SasView.[32] The wavelength of measurement was 0.8172 Å.

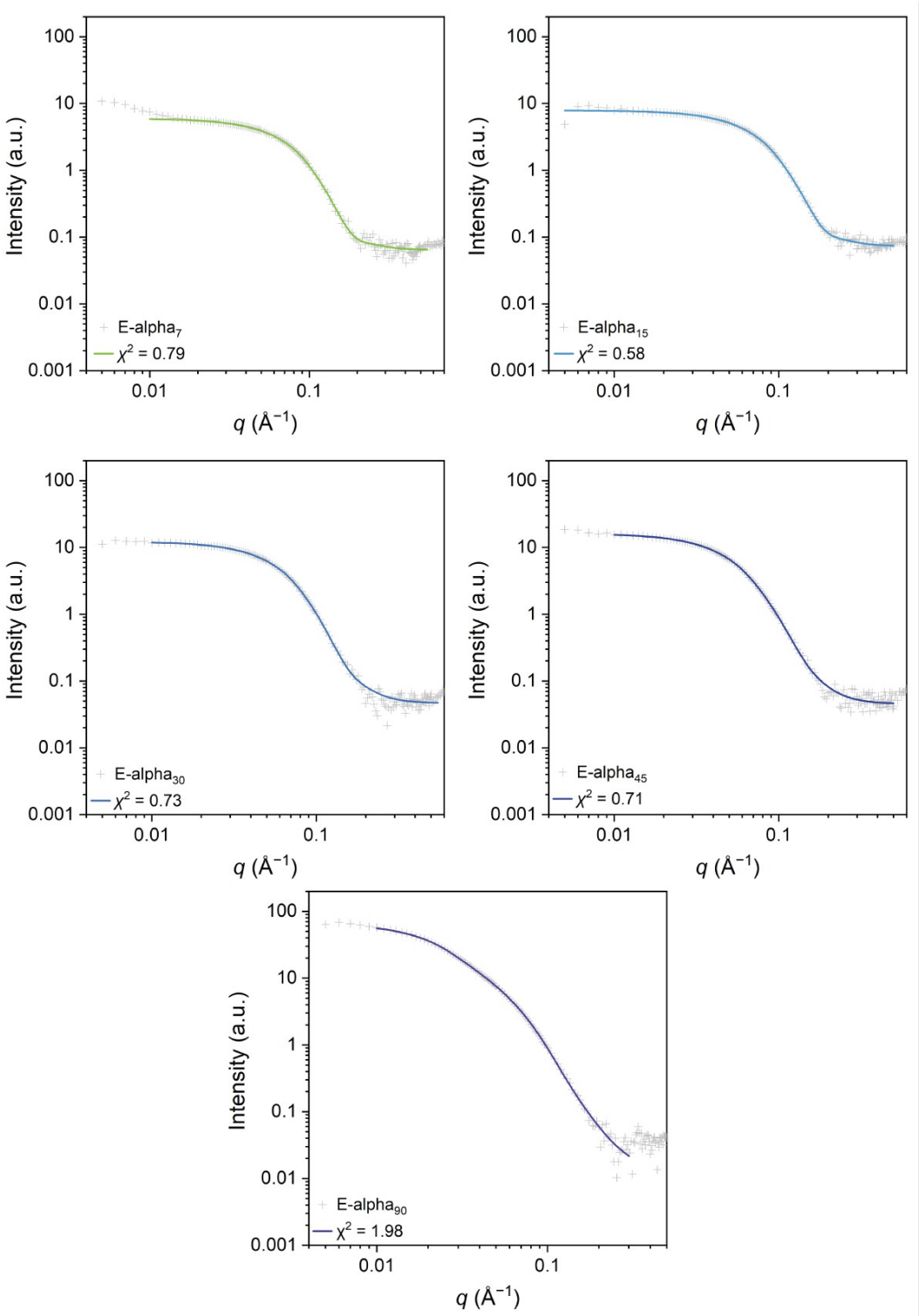

Figure S54. Background-subtracted small-angle X-ray scattering patterns of solutions of different lengths of E-alpha polymers (tick marks), with concentrations of 2.5 mg/mL in sodium carbonate buffer, compared to the flexible cylinder fits (lines) as implemented in SasView.[32] The wavelength of measurement was 0.8172 Å.

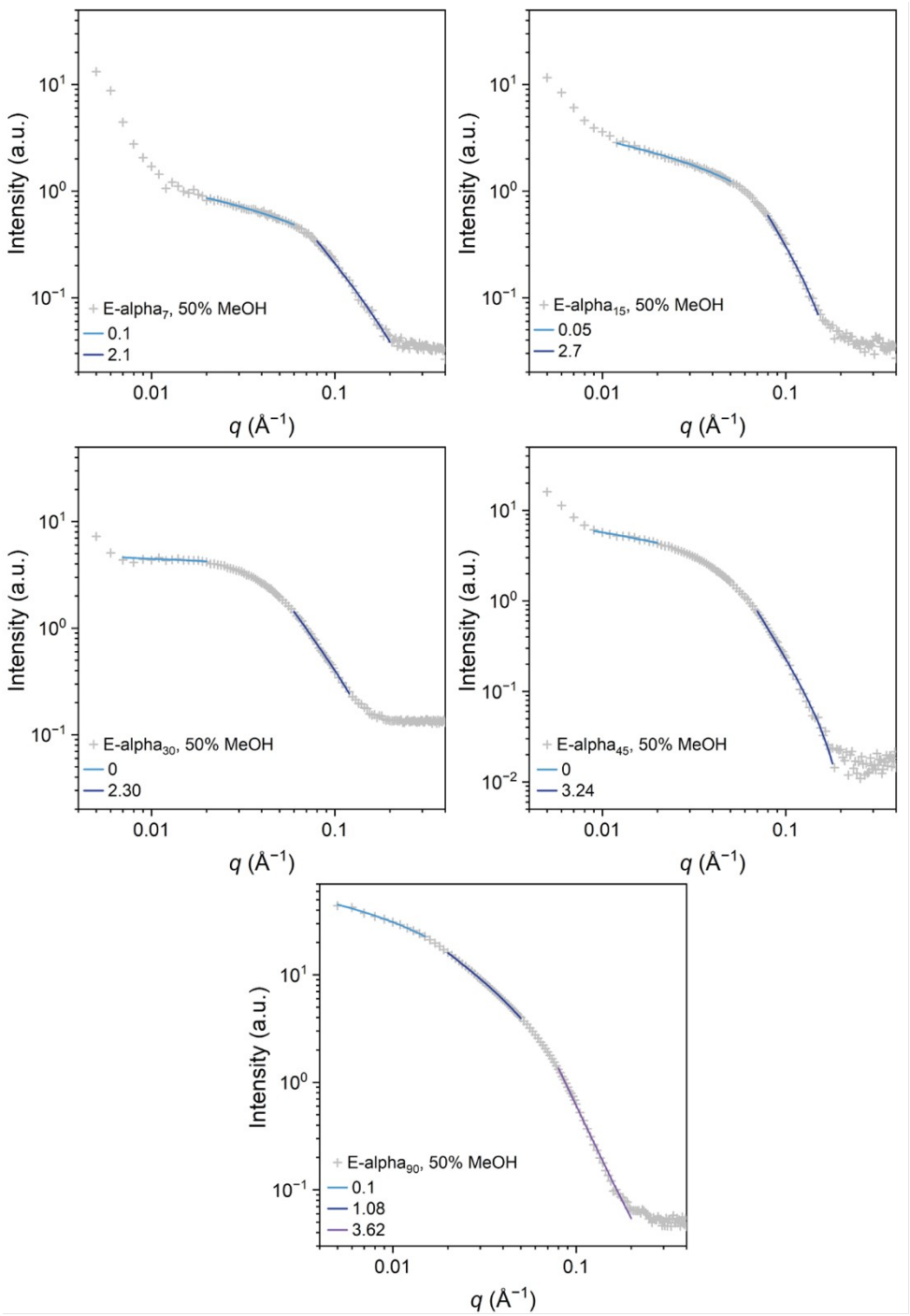

Figure S55. Background-subtracted small-angle X-ray scattering patterns of solutions of different lengths of E-alpha polymers (tick marks), with concentrations of 2.5 mg/mL in 50% MeOH, compared to the power law fits (lines) as implemented in SasView.[32] The wavelength of measurement was 0.8202 Å.

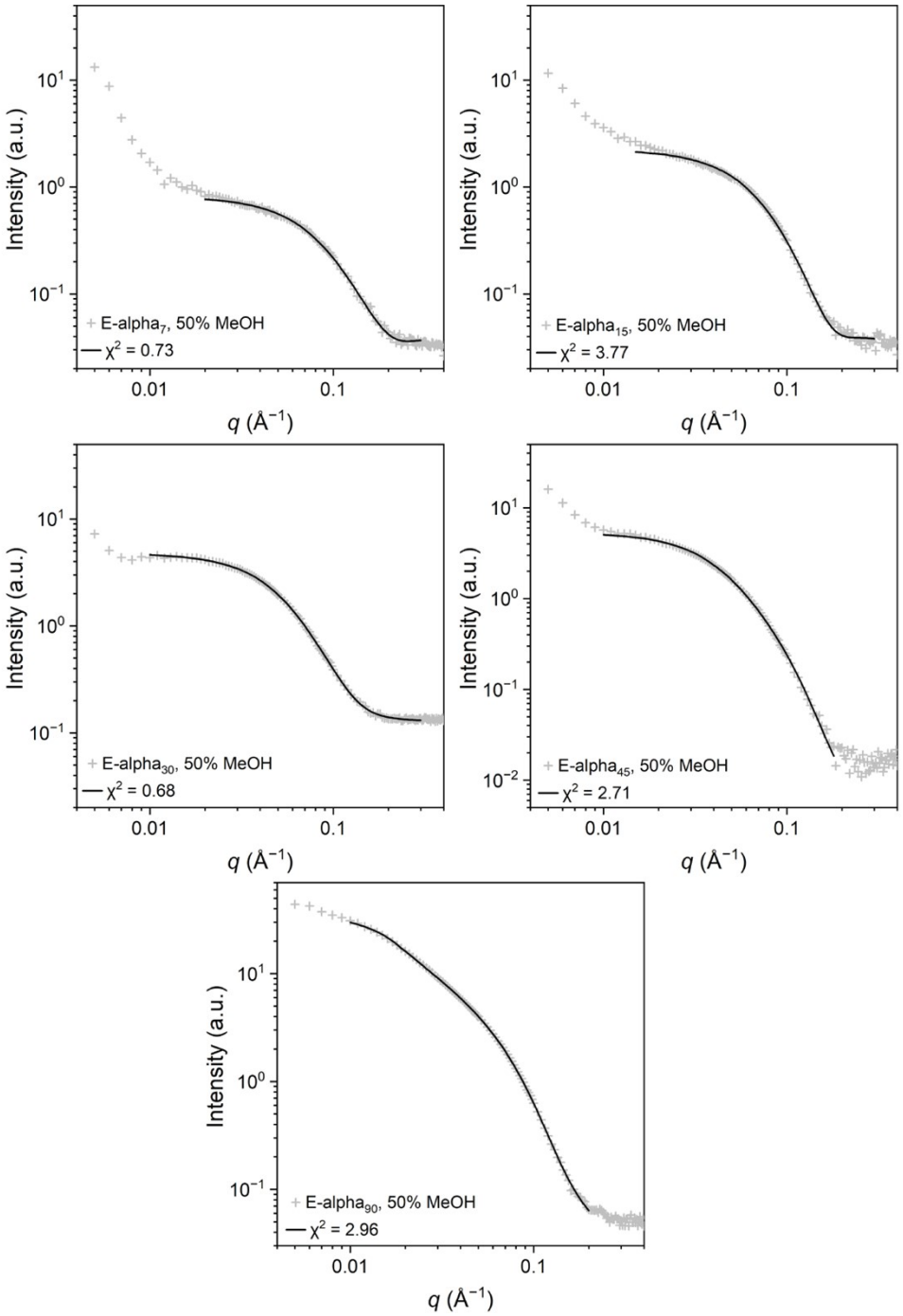

Figure S56. Background-subtracted small-angle X-ray scattering patterns of solutions of different lengths of E-alpha polymers (tick marks), with concentrations of 2.5 mg/mL in 50% MeOH, compared to the flexible cylinder model fits (lines) as implemented in SasView.[32] The wavelength of measurement was 0.8172 Å.

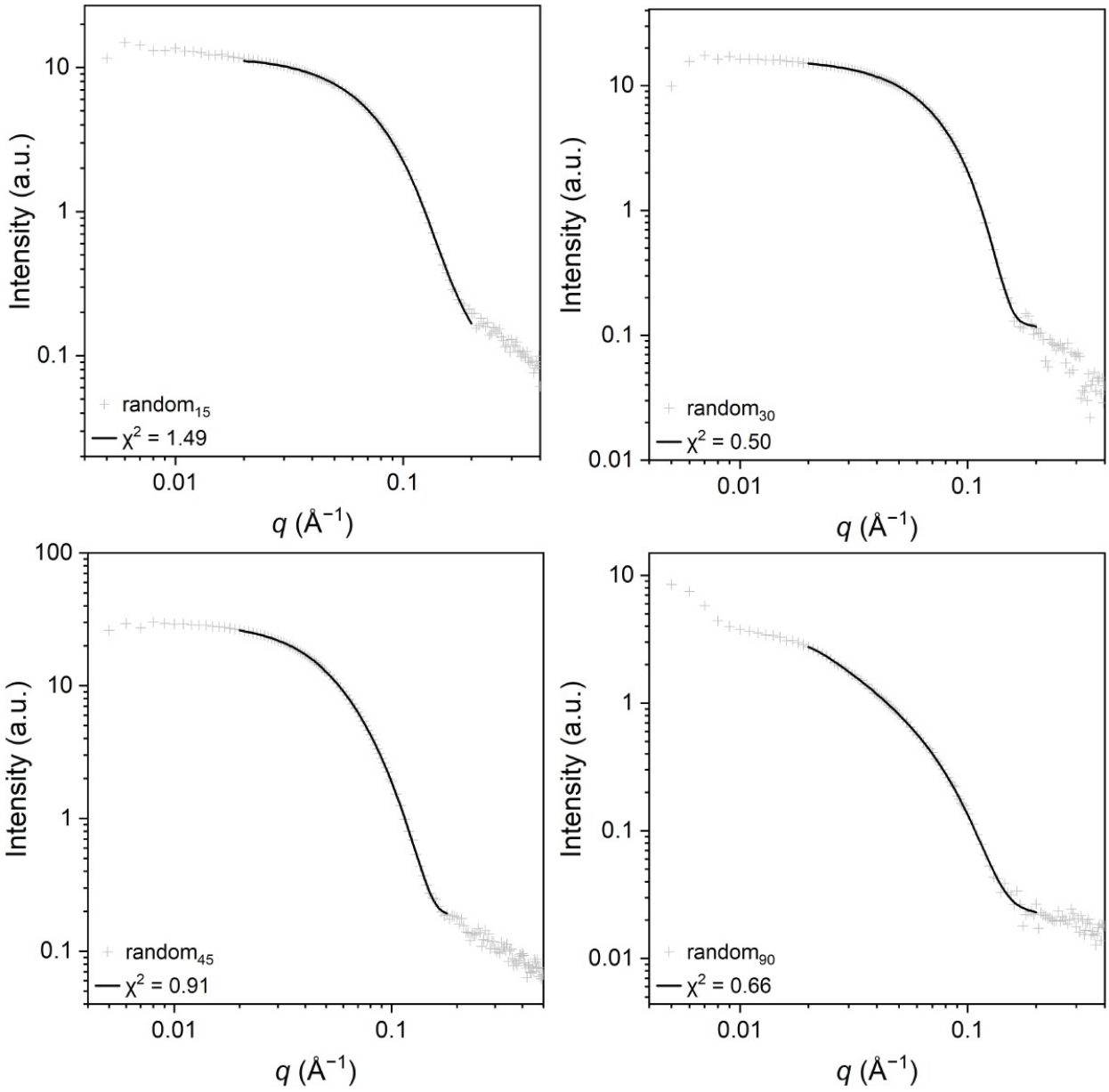

Figure S57. Background-subtracted small-angle X-ray scattering patterns of solutions of different lengths of random coil-based polymers (tick marks), with concentrations of 2.5 mg/mL in water, compared to the flexible cylinder model fits (lines) as implemented in SasView.[32] The wavelength of measurement was 0.8172 Å for all samples except random$_{90}$, which was measured with a wavelength of 0.8202 Å.

8. Cryogenic Transmission Electron Microscopy (Cryo-TEM) Measurements

For cryo-TEM measurements, 200 mesh Cu grids with a lacey carbon membrane (EMS Cat. # LC200-CU) were placed in a Pelco easiGlow glow discharger (Ted Pella Inc., Redding, CA, USA) and an atmosphere plasma was introduced on the surface of the grids for 30 s with a current of 15 mA at a pressure of 0.24 mbar. Each grid was loaded into an FEI Vitrobot Mk IV plunge

freezing system (Thermo Fisher Scientific, Waltham, MA, USA), where a 4 μL aliquot of the PLP sample (1 mg/mL, sodium carbonate buffer) was deposited onto each grid. Immediately after drop-casting, the grid was blotted for 5 seconds with a set blot force of 0.5, followed by a 0.5 second wait time before plunging into liquid ethane for vitrification. Grids were then transferred to liquid nitrogen for storage. The vitrified grids were kept under liquid nitrogen with a Gatan Cryo-Transfer Holder model 626.6 (Gatan Inc., Pleasanton, CA, USA). The imaging was performed with a JEOL JEM1400 LaB6 emission TEM (JEOL USA, Inc., Peabody, MA) operating at 120 keV equipped with a Gatan OneView CCD camera.

9. References

(1) Sandford, M. S.; Love, J. A.; Grubbs, R. H. Mechanism and Activity of Ruthenium Olefin Metathesis Catalysts. *J. Am. Chem. Soc.* **2001**, *123* (27), 6543–6554.

(2) Love, J. A.; Morgan, J. P.; Trnka, T. M.; Grubbs, R. H. A Practical and Highly Active Ruthenium-Based Catalyst That Effects the Cross Metathesis of Acrylonitrile. *Angew. Chem. Int. Ed.* **2002**, *41* (21), 4035–4037.

(3) Maynard, H. D.; Okada, S. Y.; Grubbs, R. H. Inhibition of Cell Adhesion to Fibronectin by Oligopeptide-Substituted Polynorbornenes. *J. Am. Chem. Soc.* **2001**, *123* (7), 1275–1279.

(4) Kammeyer, J. K.; Blum, A. P.; Adamiak, L.; Hahn, M. E.; Gianneschi, N. C. Polymerization of Protecting-Group-Free Peptides via ROMP. *Polym. Chem.* **2013**, *4* (14), 3929–3933.

(5) Sun, H.; Qiao, B.; Choi, W.; Hampu, N.; McCallum, N. C.; Thompson, M. P.; Oktawiec, J.; Weigand, S.; Ebrahim, O. M.; de la Cruz, M. O.; Gianneschi, N. C. Origin of Proteolytic Stability of Peptide-Brush Polymers as Globular Proteomimetics. *ACS Cent. Sci.* **2021**, *7* (12), 2063–2072.

(6) Matson, J. B.; Steele, A. Q.; Mase, J. D.; Schulz, M. D. Polymer Characterization by Size-Exclusion Chromatography with Multi-Angle Light Scattering (SEC-MALS): A Tutorial Review. *Polym. Chem.* **2023**, *15* (3), 127–142.

(7) Sreerama, N.; Woody, R. W. Estimation of Protein Secondary Structure from Circular Dichroism Spectra: Comparison of CONTIN, SELCON, and CDSSTR Methods with an Expanded Reference Set. *Anal. Biochem.* **2000**, *287* (2), 252–260.

(8) Hess, B.; Kutzner, C.; van der Spoel, D.; Lindahl, E. GROMACS 4: Algorithms for Highly Efficient, Load-Balanced, and Scalable Molecular Simulation. *J. Chem. Theory Comput.* **2008**, *4* (3), 435–447.

(9) Bonomi, M.; Branduardi, D.; Bussi, G.; Camilloni, C.; Provasi, D.; Raiteri, P.; Donadio, D.; Marinelli, F.; Pietrucci, F.; Broglia, R. A.; Parrinello, M. PLUMED: A Portable Plugin for Free-Energy Calculations with Molecular Dynamics. *Comput. Phys. Commun.* **2009**, *180* (10), 1961–1972.

(10) Barducci, A.; Bonomi, M.; Parrinello, M. Metadynamics. *WIREs Comput. Mol. Sci.* **2011**, *1* (5), 826–843.

(11) Barducci, A.; Bussi, G.; Parrinello, M. Well-Tempered Metadynamics: A Smoothly Converging and Tunable Free-Energy Method. *Phys. Rev. Lett.* **2008**, *100* (2), 1–4.

(12) Pietrucci, F.; Laio, A. A Collective Variable for the Efficient Exploration of Protein Beta-Sheet Structures: Application to SH3 and GB1. *J. Chem. Theory Comput.* **2009**, *5* (9), 2197–2201.

(13) Huang, J.; Rauscher, S.; Nawrocki, G.; Ran, T.; Feig, M.; de Groot, B. L.; Grubmüller, H.; MacKerell, A. D. CHARMM36m: An Improved Force Field for Folded and Intrinsically Disordered Proteins. *Nat. Methods* **2017**, *14* (1), 71–73.
(14) MacKerell, A. D.; Bashford, D.; Bellott, M.; Dunbrack, R. L.; Evanseck, J. D.; Field, M. J.; Fischer, S.; Gao, J.; Guo, H.; Ha, S.; Joseph-McCarthy, D.; Kuchnir, L.; Kuczera, K.; Lau, F. T. K.; Mattos, C.; Michnick, S.; Ngo, T.; Nguyen, D. T.; Prodhom, B.; Reiher, W. E.; Roux, B.; Schlenkrich, M.; Smith, J. C.; Stote, R.; Straub, J.; Watanabe, M.; Wiórkiewicz-Kuczera, J.; Yin, D.; Karplus, M. All-Atom Empirical Potential for Molecular Modeling and Dynamics Studies of Proteins. *J. Phys. Chem. B* **1998**, *102* (18), 3586–3616.
(15) Miyamoto, S.; Kollman, P. A. Settle: An Analytical Version of the SHAKE and RATTLE Algorithm for Rigid Water Models. *J. Comput. Chem.* **1992**, *13* (8), 952–962.
(16) Darden, T.; York, D.; Pedersen, L. Particle Mesh Ewald: An N ·log(N) Method for Ewald Sums in Large Systems. *J. Chem. Phys.* **1993**, *98* (12), 10089–10092.
(17) Essmann, U.; Perera, L.; Berkowitz, M. L.; Darden, T.; Lee, H.; Pedersen, L. G. A Smooth Particle Mesh Ewald Method. *J. Chem. Phys.* **1995**, *103* (19), 8577–8593.
(18) Lee, J.; Cheng, X.; Swails, J. M.; Yeom, M. S.; Eastman, P. K.; Lemkul, J. A.; Wei, S.; Buckner, J.; Jeong, J. C.; Qi, Y.; Jo, S.; Pande, V. S.; Case, D. A.; Brooks, C. L.; MacKerell, A. D.; Klauda, J. B.; Im, W. CHARMM-GUI Input Generator for NAMD, GROMACS, AMBER, OpenMM, and CHARMM/OpenMM Simulations Using the CHARMM36 Additive Force Field. *J. Chem. Theory Comput.* **2016**, *12* (1), 405–413.
(19) Carrow, K. P.; Hamilton, H. L.; Hopps, M. P.; Li, Y.; Qiao, B.; Payne, N. C.; Thompson, M. P.; Zhang, X.; Magassa, A.; Fattah, M.; Agarwal, S.; Vincent, M. P.; Buyanova, M.; Bertin, P. A.; Mazitschek, R.; Olvera de la Cruz, M.; Johnson, D. A.; Johnson, J. A.; Gianneschi, N. C. Inhibiting the Keap1/Nrf2 Protein-Protein Interaction with Protein-Like Polymers. *Adv. Mater.* **2024**, *36* (21), 1–36.
(20) Qiao, B.; De La Cruz, M. O. Enhanced Binding of SARS-CoV-2 Spike Protein to Receptor by Distal Polybasic Cleavage Sites. *ACS Nano* **2020**, *14* (8), 10616–10623.
(21) Du, F.; Rische, C. H.; Li, Y.; Vincent, M. P.; Krier-Burris, R. A.; Qian, Y.; Yuk, S. A.; Almunif, S.; Bochner, B. S.; Qiao, B.; Scott, E. A. Controlled Adsorption of Multiple Bioactive Proteins Enables Targeted Mast Cell Nanotherapy. *Nat. Nanotechnol.* **2024**.
(22) Jiang, T.; Hall, A.; Eres, M.; Hemmatian, Z.; Qiao, B.; Zhou, Y.; Ruan, Z.; Couse, A. D.; Heller, W. T.; Huang, H.; de la Cruz, M. O.; Rolandi, M.; Xu, T. Single-Chain Heteropolymers Transport Protons Selectively and Rapidly. *Nature* **2020**, *577* (7789), 216–220.
(23) L., M. R. S. MestRe Nova. 2022.
(24) Yang, L.; Antonelli, S.; Chodankar, S.; Byrnes, J.; Lazo, E.; Qian, K. Solution Scattering at the Life Science X-Ray Scattering (LiX) Beamline. *J. Synchrotron Radiat.* **2020**, *27* (LiX), 804–812.
(25) Difabio, J.; Chodankar, S.; Pjerov, S.; Jakoncic, J.; Lucas, M.; Krywka, C.; Graziano, V.; Yang, L. The Life Science X-Ray Scattering Beamline at NSLS-II. *AIP Conf. Proc.* **2016**, *1741*.
(26) Yang, L.; Lazo, E.; Byrnes, J.; Chodankar, S.; Antonelli, S.; Rakitin, M. Tools for Supporting Solution Scattering during the COVID-19 Pandemic. *J. Synchrotron Radiat.* **2021**, *28*, 1237–1244.
(27) Manalastas-Cantos, K.; Konarev, P. V.; Hajizadeh, N. R.; Kikhney, A. G.; Petoukhov, M.

V.; Molodenskiy, D. S.; Panjkovich, A.; Mertens, H. D. T.; Gruzinov, A.; Borges, C.; Jeffries, C. M.; Sverguna, D. I.; Frankea, D. ATSAS 3.0: Expanded Functionality and New Tools for Small-Angle Scattering Data Analysis. *J. Appl. Crystallogr.* **2021**, *54*, 343–355.

(28) Hammouda, B. A New Guinier–Porod Model. *J. Appl. Crystallogr.* **2010**, *43* (4), 716–719.

(29) Hammouda, B. Analysis of the Beaucage Model. *J. Appl. Crystallogr.* **2010**, *43* (6), 1474–1478.

(30) Pedersen, J. S.; Schurtenberger, P. Scattering Functions of Semiflexible Polymers with and without Excluded Volume Effects. *Macromolecules* **1996**, *29* (23), 7602–7612.

(31) Chen, W. R.; Butler, P. D.; Magid, L. J. Incorporating Intermicellar Interactions in the Fitting of SANS Data from Cationic Wormlike Micelles. *Langmuir* **2006**, *22* (15), 6539–6548.

(32) Doucet, M.; Cho, J. H.; Alina, G.; Attala, Z.; Bakker, J.; Bouwman, W.; Bourne, R.; Butler, P.; Cadwallader-Jones, I.; Campbell, K.; Cooper-Benun, T.; Durniak, C.; Forster, L.; Gilbert, P.; Gonzalez, M.; Heenan, R.; Jackson, A.; King, S.; Kienzle, P.; Krzywon, J.; Maranville, B.; Murphy, R.; Nielsen, T.; O'Driscoll, L.; Potrzebowski, W.; Prescott, S.; Ferraz Leal, R.; Rozyczko, P.; Snow, T.; Washington, A.; Wolf, C. SasView Version 5.0.5. Zenodo June 2022.

(33) Wei, Y.; Hore, M. J. A. Characterizing Polymer Structure with Small-Angle Neutron Scattering: A Tutorial. *J. Appl. Phys.* **2021**, *129* (17).

(34) Kruger, A. G.; Brucks, S. D.; Yan, T.; Cárcarmo-Oyarce, G.; Wei, Y.; Wen, D. H.; Carvalho, D. R.; Hore, M. J. A.; Ribbeck, K.; Schrock, R. R.; Kiessling, L. L. Stereochemical Control Yields Mucin Mimetic Polymers. *ACS Cent. Sci.* **2021**, *7* (4), 624–630.

(35) Pesek, S. L.; Li, X.; Hammouda, B.; Hong, K.; Verduzco, R. Small-Angle Neutron Scattering Analysis of Bottlebrush Polymers Prepared via Grafting-through Polymerization. *Macromolecules* **2013**, *46* (17), 6998–7005.

(36) Pesek, S. L.; Xiang, Q.; Hammouda, B.; Verduzco, R. Small-Angle Neutron Scattering Analysis of Bottlebrush Backbone and Side Chain Flexibility. *J. Polym. Sci. Part B Polym. Phys.* **2017**, *55* (1), 104–111.

(37) Nguyen, H. V. T.; Jiang, Y.; Mohapatra, S.; Wang, W.; Barnes, J. C.; Oldenhuis, N. J.; Chen, K. K.; Axelrod, S.; Huang, Z.; Chen, Q.; Golder, M. R.; Young, K.; Suvlu, D.; Shen, Y.; Willard, A. P.; Hore, M. J. A.; Gómez-Bombarelli, R.; Johnson, J. A. Bottlebrush Polymers with Flexible Enantiomeric Side Chains Display Differential Biological Properties. *Nat. Chem.* **2022**, *14* (1), 85–93.

(38) Yablon, L. M.; Sanders, S. N.; Li, H.; Parenti, K. R.; Kumarasamy, E.; Fallon, K. J.; Hore, M. J. A.; Cacciuto, A.; Sfeir, M. Y.; Campos, L. M. Persistent Multiexcitons from Polymers with Pendent Pentacenes. *J. Am. Chem. Soc.* **2019**, *141* (24), 9564–9569.

(39) Riback, J. A.; Bowman, M. A.; Zmyslowski, A. M.; Plaxco, K. W.; Clark, P. L.; Sosnick, T. R. Commonly Used FRET Fluorophores Promote Collapse of an Otherwise Disordered Protein. *Proc. Natl. Acad. Sci. U. S. A.* **2019**, *116* (18), 8889–8894.

(40) Riback, J. A.; Bowman, M. A.; Zmyslowski, A. M.; Knoverek, C. R.; Jumper, J. M.; Hinshaw, J. R.; Kaye, E. B.; Freed, K. F.; Clark, P. L.; Sosnick, T. R. Innovative Scattering Analysis Shows That Hydrophobic Disordered Proteins Are Expanded in Water. *Science* **2017**, *358* (6360), 238–241.